National Technical University of Athens

Department of Naval Arcitecture and Marine Engineering

Shipbuilding Technology Laboratory

Corrosion Thickness Loss Monitoring in Marine Plates through Probabilistic Methods

Diploma Thesis

of

Ilias Makras

Supervised by

Konstantinos N. Anyfantis, Assistant Professor

Athens, September 2023

Acknowledgments

This work is the final assignment for the completion of my studies at the School of Naval Arcitecture and Marine Engineering. These academic years have been pivotal in shaping both my personal and professional trajectory. I leave this school grateful for everything I learned, the moments I experienced, the friends I made and the people I met. This thesis would not have been possible without the support I received from numerous individuals.

First, I would like to express my sincere gratitude towards my thesis supervisor, Assistant Professor Konstantinos Anyfantis, for providing me with exceptional guidance and for acting in a highly professional manner. His knowledge on the subject and his desire to share it, his patience and willingness to provide assistance at all times and his deep intuitions proved invaluable during the course of this thesis. But most importantly, his moral principles and human qualities proved to be the keystone of a successful and prosperous collaboration.

In addition, words cannot express my gratitude to Ph.D. candidate, Nicholas Silionis for his enormous contribution to the completion of this thesis through his assistance and advice, and for always taking the time to have insightful discussions with me about the fascinating fields involved in my work. Always insightful, he never failed to praise my efforts and offer constructive criticism.

I would also like to thank my thesis committee, which consisted of Professor Manolis Samouilidis and Associate Professor George Dimopoulos for offering their scientific expertise for the evaluation of my thesis.

To my friends, I express my appreciation for all the experiences and memories we shared during these past years and for their understanding towards this challenging period of my life. Special thanks to my good friend, Vasiliki, with whom a great amount of my time was spent in discussing interesting topics on our field.

And last but not least, I want to express my deepest gratitude to my parents, Afroditi and Nikos, and my sister, Aggeliki, for their unconditional love and support throughout my life.

Ilias Makras

Athens, 2023

Abstract

Over the years, the practices that are used to ensure structural integrity and operational safety in the maritime sector have remained basically the same; and although efficient, they present some important drawbacks. In looking to enable a shift towards predictive and condition-based maintenance, the field of Structural Health Monitoring (SHM) has emerged as a viable option among stakeholders. The goal of SHM is to infer the existence or level of structural degradation using large amounts of in situ sensor-obtained data. In this direction, the objective of this study is to construct a SHM system that estimates the thickness loss due to corrosion in the marine operational environment utilizing strain sensing. For this purpose, a simple rectangular plate at uniform corrosion was considered as a reference structural element, which was subjected to stochastic loading as well. The quantity of interest was treated in a probabilistic framework using Bayesian inference. Strain response data were produced through a high-fidelity Finite Element (FE) model and due to the nature of Bayesian updating, surrogate models were employed to proceed to solution efficiently.

Keywords: Structural Health Monitoring, uncertainty quantification, inverse problem, Bayesian inference, strain sensing.

Περίλιψη

Τα τελευταία χρόνια, οι πρακτικές που χρησιμοποιούνται για να διασφαλιστεί η κατασκευαστική ακεραιότητα και η λειτουργική ασφάλεια στον ναυτιλιακό τομέα έχουν παραμείνει ουσιαστικά ίδιες· και αν και αποδοτικές, παρουσιάζουν κάποια σημαντικα μειονκτήματα. Επιδιώκοντας μια μεταβολή προς την προγνωστική και υπο συνθήκες συντήρηση, ο τομέας της Παρακολούθησης Δομικής Ακεραιότητας (ΠΔΑ) κατασκευών εχει αναδειχθεί ως βιώσιμη επιλογή απο τα ενδιαφερόμενα μέρη του τομέα. Ο στόχος των συστημάτων ΠΔΑ είναι η εξαγωγή συμπερασμάτων σχετικά με την ύπαρξη ή τον βαθμό δομικής υποβάθμισης, χρησιμοποιώντας μεγάλες ποσότητες δεδομένων απο επιτόπιους αισθητήρες. Προς αυτή την κατεύθυνση, ο σκοπός αυτής της εργασίας είναι να κατασκευάσει ενα σχέδιο ΠΔΑ, το οποίο να εκτιμάει την απώλεια πάχους λόγω διάβρωσης στο ναυτιλιακό περιβάλλον λειτουργείας, χρησιμοποιώντας ανίχνευση παραμορφώσεων. Για τον σκοπό αυτό, θεωρήθηκε μια απλή ορθογώνια πλάκα σε συνθήκες ομοιόμορφης διάβρωσης, η οποία υποβάλλεται μάλιστα σε στοχαστική φόρτιση. Ο χειρισμός της ποσότητας ενδιαφέροντος έγινε σε πλαίσιο πιθανοτήτων χρησιμοποιώντας Μπεϋζιανή συμπερασματολογία. Τα δεδομένα παραμορφωσιακής απόκρισης δημιουργήθηκαν μέσω ενός μοντέλου Πεπερασμένων Στοιχείων (ΠΣ) υψηλής ακρίβειας και λόγω της φύσης της Μπεϋζιανής αναβάθμισης πληροφορίας, υποκατάστατα μοντέλα χρησιμοποιήθηκαν για την επίτευξη της λύσης αποδοτικά.

Λέξεις κλειδιά: Παρακολούθηση Δομικής Ακεραιότητας, ποσοτικοποίηση αβεβαιότητας, αντίστροφο πρόβλημα, Μπεϋζιανή συμπερασματολογία, αισθητήρες παραμορφώσεων.

Table of Contents

List of Figures

List of Tables

Abbreviations

Autocorrelation Function	ACF
Condition-based Maintenance	CBM
Corrosion Induced Thickness Loss	CITL
Digital Twin	DT
Degrees of Freedom	DOFs
Finite Element Analysis	FEA
Finite Element Method	FEM
International Association of Classification Societies	IACS
International Maritime Organization	IMO
Markov Chain Monte Carlo	MCMC
Metropolis Hastings	MH
Monte Carlo	MC
Monte Carlo Simulation	MCS
Non-Destructive Evaluation/Testing	NDE/NDT
Physical Twin	PT
Probability Density Function	PDF
Quantity of Interest	QoI
Structural Health Monitoring	SHM
Uncertainty Quantification	UQ

1 Introduction

1.1 Current State of Damage Identification Practices

Preservation of structural integrity is a challenging task for infrastructure systems with geometry- and operational-level complexities, such as ships, offshore and land-based structures. The most common and effective practices to ensure the safe operation of a structure have remained unchanged over the better part of modern engineering history. These practices essentially are: a) significantly overcompensating for vaguely defined potential loading scenarios, usually of stochastic nature as well as uncertainty regarding the material, and b) planning ahead for normal wear. This is especially the case in the highly unpredictable and corrosive environment where ships and marine structures operate. In addition to conservative design, periodical surveys and maintenance are required throughout the life cycle of a structure. In the maritime industry, current practices involve strict preventive maintenance schemes centered around temporally fixed inspections that are imposed by the International Maritime Organization (IMO) and overseen by classification societies. Damage identification is based on visual inspection and non-destructive evaluation (NDE) carried out on site in predetermined minimum time intervals. Due to the vast number of structural elements a ship is composed of, surveys focus on designated areas and structural details that are expected to be corroded or are susceptible to certain types of failure [1].

In Figure 1.1 the sketch of a transverse section of a typical dry cargo vessel is depicted. Marked on it are notes and comments regarding damage modes most frequently occurring on each of the designated locations. This figure is provided in a relevant report of recommendations regarding the inspection of bulk carriers and tankers, published by the International Association of Classification Societies (IACS).
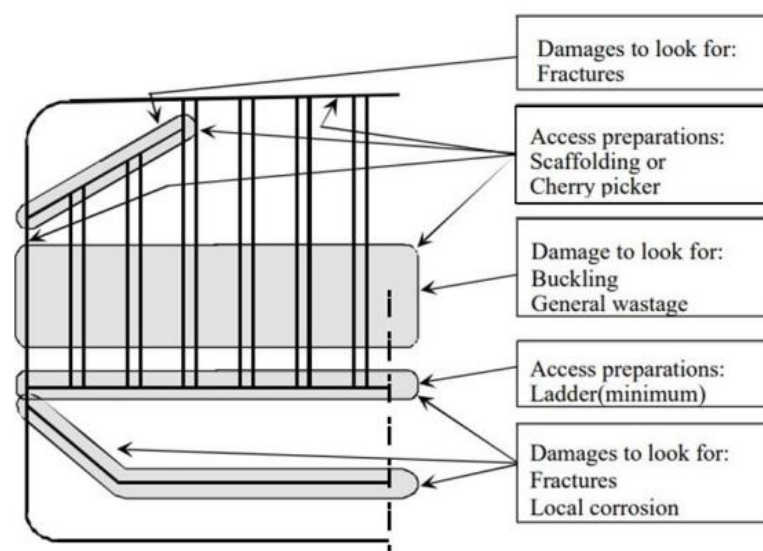
Figure 1.1: Sketch of transverse bulkhead with instructions for damage inspection as recommended by IACS guidelines. (Source: [1]).

In the maritime operational environment, one of the prevalent types of damage is corrosion induced thickness loss (CITL). This type of damage is part of the normal

operational wear of marine structures for which structural guidelines [2] require the addition of excess thickness to structural members. Common modes of corrosion involve uniform corrosion of extensive areas as well as pitting. Pitting is a type of localized corrosion that takes the form of small craters of variable size and geometry on the material. Usually, those craters are concentrated around specific locations forming a damaged area resembling locally contained uniform corrosion [3]. This mode of corrosion, along with uniform thickness loss is prevalent on plates in the marine environment. Typically, the material addition to plates required by guidelines [2] for safe design against corrosion constitutes 20% of the nominal plate thickness. The nominal thickness is also dictated by the guidelines to ensure safe operation under expected loading conditions during the lifespan of the structure.

Due to scale, time and access constraints, inspection practitioners typically perform visual examinations on the aforementioned damage-prone locations. If the visual method does not suffice, a suitable Non-Destructive Testing (NDT) technique is deployed on site for a more refined assessment. The current NDT methods that dominate the field can be classified into three main categories; namely, enhanced visual and radiographic, acoustic and magnetic techniques [4]. Once structural damage has been identified by means of the employed inspection method, the operator must determine whether or not appropriate repair/renewal and maintenance should be performed. Selecting a suitable repair alternative involves a great deal of judgment and engineering insight and is typically a trade-off between robustness and cost.

However, the aforementioned methods have many drawbacks. Firstly, human intervention is required. On top of that, the inspector is required to be highly skilled with great expertise and pass high qualification standards in order to ensure correct evaluation of the readings. Techniques require that the vicinity of the damage is known a priori and that the portion of the structure being inspected is readily accessible. Prevention is based on statistically locating faults by sample tests throughout the structure, focusing on areas susceptible to damage. Additionally, most methods are limited to detection of damage on or near the surface of the structure [5]. Moreover, NDE is applied on a single damage instance, at a specific timeframe. No information is gained about the evolution of the damage when operation continues, or the overall health of the structure given the presence of the damage.

Furthermore, in order to transition to more environmentally and economically sustainable structures, it is required to reduce material wastage. It would be of immediate benefit to work components closer to failure rather than preventively replacing them because of uncertainty about their remaining operational reliability. The aforementioned issues illustrate the need for a shift into a more holistic and proactive approach to maintenance, i.e., Condition-based Maintenance (CBM). Essentially, CBM recommends maintenance actions (i.e., decisions) based on data gathered through a process of condition monitoring allowing operators to gain access to salient benefits [6]. Weighed against preventive maintenance, the primary advantages CBM offers are the increased system reliability as well as the significant cost savings due to the reduced material wastage and the decreased mean downtime as a result of less reliance on periodic inspections. The next section delves into the concepts of Digital Twin (DT)

and Structural Health Monitoring (SHM), which both play an increasingly important role in the realization of the CBM paradigm.

1.2 Digital Twin and Structural Health Monitoring

From a practical perspective, a DT can be defined as the computerized companion of a real-world physical asset, i.e., the Physical Twin (PT), intended to serve as a dynamic and accurate replica of the PT's behavior within a target setting [7]. To ensure solid physical interpretability, the DT should be augmented with high-fidelity physics-based models, which will be constantly updated as data from permanently installed sensors on the PT and will be received in a real-time fashion. The DT can then be leveraged for conducting different "what-if" scenarios of service function (i.e., operation, inspection, etc.) for the life-cycle integrity management of the PT. The extant literature underlines many of the prospective and immediate benefits of the DT intervention in the industrial arena that accumulate to the PT's overall efficiency, including risk [8] and cost [9] reduction, security [10], resilience [11] and reliability [12] enchantment and of course decision-making assistance [13]. An overview of the digital twin as it may be implemented in shipping, along with the underlying technologies it encompasses is shown in Figure 1.2.
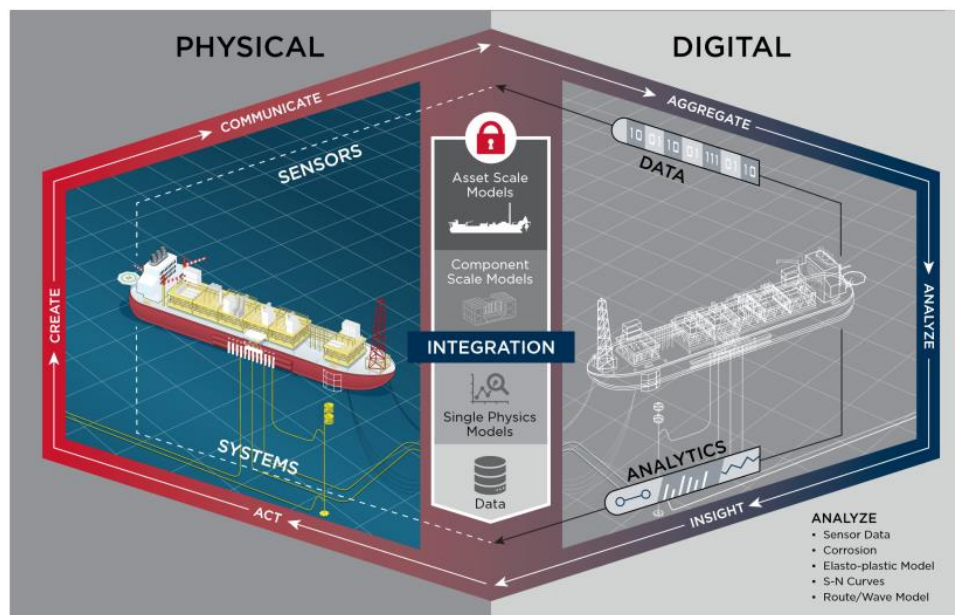
Figure 1.2: DT technology for an FPSO hull structure: Interaction between the physical space and the digital space. (Source: [14]).

However, it should be noted that relevant research and application regarding the implementations of structural digital twin in modern ocean-going vessels and offshore structures are still at an early stage. In general, research on the subject is more focused on the implementation of the principles of SHM in order to gather insights on how to approach the problem of damage detection in ship structures, thus making possible the creation of a data enabled structural digital twin [15]. Structural Health Monitoring refers to systems which enable the automatic and on-line observation of structural integrity of any given component during service [16]. However, the information is not

limited to the structural health of a system, rather it may include data regarding operational procedures, performance metrics, financial analytics and anything of interest depending on each application.

The SHM framework should not be considered just another NDE method [17]. In defense of this statement, note for example the case of an extreme event that exceeds operational specifications. In such a scenario traditional NDE methods usually require cease of operations. On the contrary, a SHM system can provide immediate feedback on the condition of the structure and assist in deciding whether operations can safely continue afterwards. Another fundamental differentiation element is that in order to apply NDE techniques, the existence of damage should already be known, while damage detection falls within the scope of SHM systems. Furthermore, NDE does not provide up-to-date information on the overall state of the structure. On the other hand, SHM refers to near real-time systems that function in parallel with the operation of the structure (DT).

In the present study, one is interested in SHM as a damage-detection strategy. This idea of SHM as a damage-detection method is described by Farrar et al [5] as the following procedure:

- Step 1: Operational evaluation
- Step 2: Data acquisition, normalization, and cleansing.
- Step 3: Feature extraction and data condensation.
- Step 4: Statistical model development for feature discrimination.

The final step may be broken down to four levels according to Rytter [18], progressively increasing in the depth of information required:

- Level 1: Detection
- Level 2: Localization
- Level 3: Characterization
- Level 4: Prediction

Plates on a marine vessel, which is the subject of analysis in this work, are required to be replaced once damage exceeds a threshold indicated by formal guidelines. Hence, focus is pointed towards only level 1 and level 3 SHM statistical model development.

As mentioned previously, in SHM, information about the structure integrity is being constantly updated using collected data. Towards this direction, one encounters Bayesian inferential statistics as powerful tool in SHM applications. One paradigm of this is the work of Zhu and Frangopol [19], where Bayesian updating is applied to assess the reliability and redundancy of a ships cross section based on load effects.

Another thing that is important to point out is that the strain response of a structure is commonly used as the source of information for SHM. A strain-based framework was utilized in recent works of Silionis et al [20] for the detection and localization of extensive damage in thin-walled structures as well as by Argyris et al [21] for Bayesian optimal sensor placement for crack identification in structures.

In the marine and offshore industry, SHM implementations are frequently discussed. Corrosion detection on ship hull structures is studied in the works by Katsoudas [17] and by Silionis et al [22] where in both a strain-based approach is implemented and in the work by Yao et al [23] where a machine-vision, image-based approach is utilized. Nonetheless, to the author's knowledge, the applications of SHM systems in the sector are still limited. One important consideration amongst the limiting factors is the lack of standardization and reliable metrics to evaluate the suggested methods [24]. SHM systems in practice are more commonly seen in offshore wind turbines as per the review of Martinez-Luengo et al [25].

1.3 Thesis Objective and Overview

In the previous sections a brief overview of the research around SHM was presented. The present thesis is inspired not only by the aforementioned ideas but also by a willingness to approach the benefits of transitioning to a condition-based maintenance scheme, which empowers the vision of increased service performance, structural integrity and safety of operation in a sustainable future for the industry. More specifically, the purpose of this study is to design an appropriate SHM scheme that will be capable of estimating the corrosion induced thickness loss in marine plates, utilizing strain measurements. The thesis is focused on designing strategies for transforming the sensor data to thickness information.

In this direction, a fictitious, plate-like structural entity was selected. The choice of this simplified structural domain extricates the analysis from the need to develop an accurate model of a real-world complex structure. Moreover, possible complicated effects of geometrical nature are avoided, hence, a more clear, direct view of parameter influence on the problem is thought to be observed which hopefully would allow for qualitative deductions to be made that could be generalized for different applications. The aforementioned plate was then subjected to a global uniform thickness reduction representing the uniform corrosion due to the operational environment of marine structures. Strain response data are obtained from a high-fidelity FE model.

A kye challenge in modeling naval structures is the stochastic nature of their operational profile. The marine environment is modeled in a probabilistic manner, thus, designing and studying models in determined loading scenarios may not be representative of the real world. In the present study high operational variability was modeled in the input by introducing several parameters as random variables. The structural domain was considered to be subjected to distributed pressure loads of random peak magnitude and location.

This inherent probabilistic nature of reality poses a corresponding uncertainty to the quantity of interest (QoI), i.e., the remaining from corrosion, thickness of the plate. The aim of this thesis is not limited to just point estimate this thickness. It is equally important to quantify this associated uncertainty that describes this parameter. It is important to note that the QoI and the observable data are only indirectly connected through a deterministic forward model, thus posing an inverse uncertainty quantification problem. Towards the direction of inverse uncertainty quantification, Bayesian statistics were considered the most appropriate approach since the QoI is

treated from the beginning as random variable and thus in a probabilistic manner. To proceed to the solution of the Bayesian problem Markov Chain Monte Carlo (MCMC) algorithm was employed. Due to the iteration nature of the aforementioned algorithm, surrogate models were necessary to proceed to solution efficiently.

The following chapters elaborate on the aforementioned topics and explain in depth the concepts applied and the steps taken towards accomplishing the objective of this thesis. Chapter 2 provides some insight regarding the framework around the concepts included in this study. In Chapter 3 the development of the problem at hand is described followed by the details on the FE modeling procedure. Chapter 4 describes the procedure of selecting the optimal sensor features. In chapter 5 the probabilistic model is constructed along with surrogate modeling. Chapter 6 contains the results of Bayesian inference and finally, chapter 7 summarizes this analysis, offers some final thoughts around the subject and provides inspiration for extensions in the future.

2 Theoretical Background

The introduction provided a first look into the ideas that inspired this work and a general overview of the procedures executed for the purposes of the present study. The aim of the current section is to present in theoretical terms the basic concepts and tools of analysis tied with the technical portion of this thesis. In this regard, by the end of this chapter, the reader should have a solid understanding of the concepts such as Uncertainty Quantification (UQ) in inverse problems, Bayesian Statistics, Markov Chain Monte Carlo methods (MCMC), Surrogate Modeling and Finite Element Method. The advanced reader can be directed to the literature referred along each subject for more specialized and holistic information.

2.1 Uncertainty Quantification (UQ)

Uncertainty quantification (UQ) is the process of quantifying and analyzing the uncertainty in mathematical models, simulations and data. The primary aim is to assess the reliability of predictions, account for the effects of variability, randomness and misspecification in models, and ultimately assist in decision-making. UQ is an increasingly important interdisciplinary field which combines statistical, computational and mathematical methods to estimate, propagate and bound the uncertainty in models.

2.1.1 Sources and Types of Uncertainty

There is no argument that structural systems are subject to a multitude of uncertainty sources. There are two primary classifications of uncertainty; namely, aleatoric and epistemic [26]. Aleatoric uncertainty is a type of uncertainty that originates from the unavoidable inherent randomness or variability in the system being modelled or measured. It is also referred to as stochastic or random uncertainty. Aleatoric uncertainty in engineering problems may become present in structural loads, as well as in material properties, structural dimensions (scantlings), and fabrication-related geometric tolerances, just to mention a few. Errors associated with the deployed data acquisition system (e.g., measurements noise, sensor misplacements, etc.) also fall under this category. Essentially, inherent variability is a state of nature, and the accompanying uncertainty is irreducible. In contrast epistemic uncertainty is the type of uncertainty that arises from the limited knowledge, data, or information available about the system being modelled or measured. Foremost among the sources of epistemic uncertainty is the prediction error related to the computational modeling procedures that have gained popularity in the last decades for several applications of practical interest in science and engineering. Theoretically, the uncertainty associated with these types of errors can be reduced by employing better physical-mathematical models or gathering additional data. Whilst aleatoric and epistemic uncertainty are referred to as two distinct classes, in practice, they often come together. This combined uncertainty is referred to as hybrid uncertainty.

2.1.2 Engineering Model

In the context of UQ, a model of an engineering system is a mathematical representation or computational simulation of the relevant physical processes. For given parameters

$x \in D_x$ from the domain $D_x \subseteq \mathbb{R}^M$ with $M \in \mathbb{N}_{>0}$, the model predicts an output of interest $\tilde{y} \subseteq \mathbb{R}$. A single response quantity is considered here for the sake of simplicity. The extension to multivariate outputs is straightforward, though. Accordingly, the model can be thought of a scalar-valued function:

$$\mathcal{M}: D_x \to \mathbb{R}$$

$$x \mapsto \tilde{y} = \mathcal{M}(x) \qquad\qquad \text{Eq. 2.1}$$

Many different types of such predictive models are encountered in engineering problems. This includes simple analytic expressions as well as numerical solutions of governing equations. Especially in the latter case, the model symbolized in Eq. 2.1 is often treated as a *black-box* i.e. it is only evaluated in a pointwise manner. Its internal structure may be unknown, too complex or simply considered explicitly. The only requirement is that the model is available in executable form. This type of model will be employed in the present study using finite element and surrogate modeling.

2.1.3 Forward and Inverse Problems

Broadly speaking, based on the engineering model described in section 2.1.2, UQ problems can be divided into forward UQ problems, i.e. characterizing the model outputs, and inverse UQ problems, i.e. learning about the model inputs. See Figure 2.1 for visualization. A typical example of forward UQ problem is uncertainty propagation [27]. In uncertainty propagation one tries to quantify the influence of input parameter uncertainty on the predictions of the engineering model. By representing the uncertain inputs as random variables with a prespecified probability distribution, the problem becomes to characterize the corresponding output distribution. These types of problems are usually treated using conventional Monte Carlo methods [28]. Forward UQ problems also include reliability analysis where one focuses on the computation of the failure probability, e.g. that the system output exceed a certain threshold. However, the problem of interest in this study is model parameter estimation. Parameter estimation belongs to inverse UQ problems. In an inverse problem, one is given noisy observations of the system output and the goal is to estimate the unknown system input parameters and their corresponding uncertainties. The quantities that interest focuses on and the ones that can be observed are only indirectly connected through a deterministic forward model like the one in Eq. 2.1.
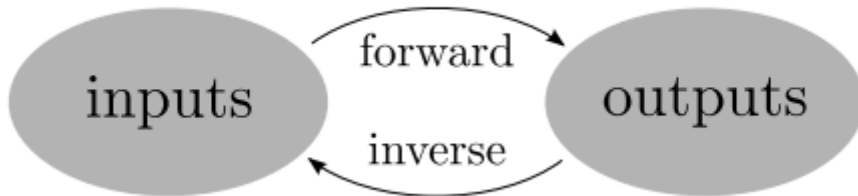
Figure 2.1: Forward and inverse problems. (Source: [29])

The main issue when dealing with inverse UQ problems is that they are typically ill-posed. A problem is called well-posed after Hadamard if the existence, uniqueness and

stability of a solution are given. Physical forward problems are often well-posed in this sense. In contrast, in the case of inverse problems, the measurement noise, the inability of the forward model to be inverted and a lack of data lead to ill-posedness. When a problem is ill-posed, a solution may be neither existent nor unique, moreover, it may not be continuously dependent on the data. For that reason, one cannot apply the conventional Monte Carlo methods in inverse problems. The standard numerical methods that cope with the issue of ill-posedness are the so-called regularization methods [30]. Another way to deal with inverse UQ problems is Bayesian inference. Bayesian inference establishes a probabilistic framework that allows one to coherently quantify uncertainties with due regard to all available information. It is based on the transition of a prior into a posterior probability distribution reflecting the learning process. Basically, the prior and the posterior represent the state of knowledge or level of uncertainty before and after incorporating the experimental observations. A thorough insight on how Bayesian inference is applied in inverse UQ problems will be presented in the next section. Regarding the issue of ill-posedness, Stuart [31] transferred Hadamard's principle of well-posedness to Bayesian inverse problems: the posterior exists, it is unique, and it is locally Lipschitz continuous with respect to the data.

2.2 Bayesian Inference

2.2.1 General

In the field of statistical analysis, there are two main competing philosophies; namely, the frequentist and the Bayesian [32]. Frequentist approach to statistical inference is also known as classical approach since it is being applied more widely by statisticians throughout the years. Regarding the Bayesian approach, although its origin is dated around the 18th century, the associated computational complexity limited its application. However, the current increasing power of computers is bringing Bayesian methods to the fore.

The main differences between the frequentist and Bayesian approach lay on the interpretation of probability and the treatment of the parameters that need to be inferred. Frequentist approach interprets the probability of an event as the limit of the relative frequency with which the event occurs, in repeated trials under identical conditions. Alternatively, the Bayesian approach interpretation regards the probability as a measure of the degree of belief of the individual assessing the uncertainty of a particular event on a [0,1] scale. Furthermore, frequentist methods regard the parameters of interest as fixed, unvarying but unknown quantities whereas Bayesian methods regard these parameters as random variables and assign probability distributions to them. These probability distributions are the so-called prior distributions that basically reflect the subjective knowledge over the parameter values before considering any observations. Observing the data is then an event with respect to which the priors shall be conditioned. By applying the Baye's rule one can extract the posterior distributions of the parameters as an inference of the combination of the subjective knowledge and the observations. Treating the parameters in a probabilistic framework (as random variables), automatically reflects the uncertainty of these parameters. This distinct feature gives a great advantage to Bayesian methods over frequentist methods. Generally speaking,

frequentist methods provide point estimations for the parameters (see the method Maximum Likelihood Estimation [33]) and fail to quantify statistical uncertainties, which is something that Bayesian methods are capable of doing.

2.2.2 Likelihood Function

In the following, the unknown parameters of the statistical model are denoted as $x = (x_1, \ldots, x_K)^T \in \mathbb{R}^M$. The number of the unknown is denoted as $M \in \mathbb{N}_{>0}$ which is in line with the notation of the preceding section. To proceed to the statistical identification of the unknown parameters, $N \in \mathbb{N}_{>0}$ real measurements $y = (y_1, \ldots, y_N)^T \in \mathbb{R}^N$ are extracted. In order to draw inferences from the data y about the unknowns x, one has to establish the connection between them. Therefore, one constructs a probabilistic model $p(y|x)$ that explains the randomness of the data for given parameter values. This is often denoted as:

$$Y|x \sim p(y|x) \qquad \text{Eq. 2.2}$$

In this way the actually acquired data are interpreted as random realization $Y = y$ generated from Eq. 2.2 for the true values of the unknowns. This probabilistic model represents the likelihood function of the model, and it plays a key role in Bayesian inference [34]. For the obtained fixed observations y the likelihood function is defined as:

$$\mathcal{L}(x|y) = p(y|x) \qquad \text{Eq. 2.3}$$

Hence, the likelihood emerges from evaluating the conditional density in Eq. 2.2 as a function of the unknowns x. It is remarked that while the form of $\mathcal{L}(x|y)$ is seemingly simple, it embodies a variety of assumptions and simplifications that are made during the modeling process. Even the notions of true parameter values and a data generating mechanism can be seen as conceptualization. Further information on how such a statistical model will be constructed in connection with the inverse problem will be discussed in Chapter 5.

It is also noted that, for N independent observations y the likelihood function becomes the product:

$$\mathcal{L}(x|y) = \prod_{i=1}^{N} p(y_i|x) \qquad \text{Eq. 2.4}$$

2.2.3 Prior Distribution

As mentioned before, the Bayesian approach to inference and prediction is built on probabilistic reasoning, involving a subjective interpretation of probability and randomness to the unknown parameters x. This way it allows for more thorough information processing and uncertainty analysis. The modeler's and analyst's ignorance regarding the true parameter values before analyzing the data is represented as a random vector:

$$X \sim \pi(x) \hspace{4cm} \text{Eq. 2.5}$$

Here, $\pi(x)$ is called the prior distribution. In essence, instead of acknowledging the fact that the parameter values are not known, their uncertainty is modeled as a probability distribution. The true values are considered a realization $X = x$ of the random vector in Eq. 2.5.

The selection of the prior distribution is of utmost practical importance in Bayesian inference. It is as well the most controversial aspect. On the one hand, the prior allows one to incorporate qualitative and quantitative information other than the data. Beyond physical constraints, this includes heterogenous sources such as expert knowledge, previous experiments and published literature. On the other hand, this raises the question of how to encode such information into a probability distribution. Similar to the assumptions and simplifications have to be made in order to formulate a probabilistic data model as in Eq. 2.2, the determination of the prior parameter model in Eq. 2.5 can be understood as a modeling choice.

Broadly speaking, one may classify Bayesian priors according to the way they are chosen and the information they convey. For start, one may distinguish between priors that are more subjective, i.e. elicited on the basis of one's own or someone else's personal belief [35], or more objective, i.e. constructed according to some more formal rules [36]. Subjective and objective prior distributions are also called informative and uninformative, respectively. These terms are used in order to characterize the prior with respect to its information content. There are also more or less functional priors that serve certain purposes. They are chosen for mere mathematical convenience or their regularization properties. Conjugacy [37], robustness [38] and sparsity [39] can be for instance achieved by choosing appropriate priors.

In engineering practice, one often designates a well-known family of distributions as candidate priors. The corresponding parameters are then set to as to mirror the uncertainty as faithfully as possible. Uniform distributions are often chosen for parameters that can be bounded from above and below, e.g. due to physical constraints. Gaussian or lognormal distributions are often used for parameters that are unbounded or strictly positive, respectively.

2.2.4 Posterior Distribution

All things considered, Bayesian modeling rests on the marginal distribution $\pi(x)$ of the unknown parameters in Eq. 2.5 and the conditional distribution $p(y|x)$ in Eq. 2.2. The unknowns and the data are represented as jointly random vectors:

$$(Y, X) \sim p(y, x) = p(y|x)\pi(x) \hspace{3cm} \text{Eq. 2.6}$$

This is a complete probability model of the Bayesian experiment. The true parameters and the actual data are regarded as a realization $(Y, X) = (y, x)$ of the joint random variables in Eq. 2.6. While the outcome of the data y is observed, the true parameters x remain unobserved.

Now one can synthesize the prior information and the observed data in order to estimate the unknowns. In particular, one proceeds by conditioning on the realized data. Given the likelihood function in Eq. 2.3 and the prior distribution in Eq. 2.5, the posterior probability distribution follows from the Bayes' law:

$$p(\boldsymbol{x}|\boldsymbol{y}) = \frac{\pi(\boldsymbol{x})\mathcal{L}(\boldsymbol{x}|\boldsymbol{y})}{C} \qquad \text{Eq. 2.7}$$

$$C = \int_{\mathbb{R}^M} \pi(\boldsymbol{x})\mathcal{L}(\boldsymbol{x}|\boldsymbol{y})d\boldsymbol{x} \qquad \text{Eq. 2.8}$$

The normalizing term C is a constant, independent from the parameters $\boldsymbol{x}$ such that the posterior probability distribution integrates to 1. It is usually called model evidence or marginal likelihood. In the same way as the prior represents the uncertainty about the unknowns before analyzing the data, the posterior in Eq. 2.7 summarizes the reduced uncertainty afterwards.

In Figure 2.2 the functioning of Bayesian updating is illustrated for a single quantity of interest (QoI). The prior is transformed into the posterior density, which is paralleled by a reduction of the associated uncertainty and a higher degree of probability mass localization. For the sake of clarity, both the prior and the posterior density in the sketch are Gaussian. In most but the simplest cases, however, the posterior is a complex probability distribution that may exhibit strong non-normalities and a multiplicity of modes. Multivariate posteriors often contain linear correlations and complex dependencies between the variables involved.
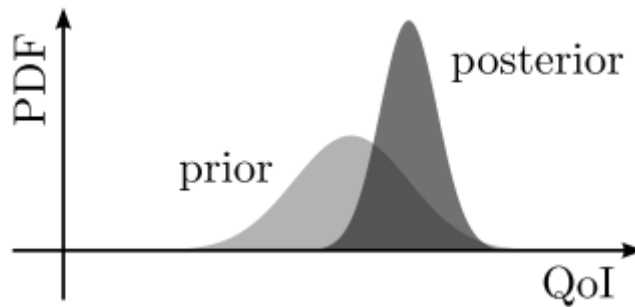
Figure 2.2: Bayesian inference. (Source: [29])

Now all information is contained in the posterior probability density function and one can proceed to the estimation of different moments of this distribution. The expected value and the covariance matrix are given as:

$$\mathbb{E}[\boldsymbol{X}|\boldsymbol{y}] = \int_{\mathbb{R}^M} \boldsymbol{x}\, p(\boldsymbol{x}|\boldsymbol{y})d\boldsymbol{x} \qquad \text{Eq. 2.9}$$

$$Cov[\boldsymbol{X}|\boldsymbol{y}] = \int_{\mathbb{R}^M} (\boldsymbol{x} - \mathbb{E}[\boldsymbol{X}|\boldsymbol{y}])(\boldsymbol{x} - \mathbb{E}[\boldsymbol{X}|\boldsymbol{y}])^T \, p(\boldsymbol{x}|\boldsymbol{y})d\boldsymbol{x} \qquad \text{Eq. 2.10}$$

The posterior mean in Eq. 2.9 is often taken as a point estimate of the unknown parameter vector, where the covariance in Eq. 2.10 is regarded as a measure of statistical uncertainty, that allows the creation of credible intervals [40].

2.3 Markov Chain Monte Carlo (MCMC)

2.3.1 Bayesian Computations

Generally, Bayesian posteriors feature an analytic closed-form expression only on a rare occasion. In order to explore the posterior distribution and to calculate the corresponding posterior moments, one needs to proceed to computational methods. The most widespread approach to computational Bayesian inference is random sampling from the posterior. However, the model evidence term in Eq. 2.7 poses an important obstacle to sampling methods, since most of the times it is computationally inefficient or even impossible to be calculated. Thus, one cannot sample directly from the posterior distribution. This is where Markov Chain Monte Carlo (MCMC) techniques come to the front. MCMC methods construct a Markov Chain that is suitable for sampling from the posterior distribution and for estimating conditional expectations. However, they only need pointwise evaluations of the unnormalized posterior density, i.e. the numerator of Eq. 2.7, and thus dispense from computing the model evidence term.

2.3.2 Monte Carlo Simulation (MCS)

MCS is a sampling-based approach that is used to compute summary statistics for a quantity of interest and evaluate its probability density. To get a better understanding of the approach, consider the engineering model of Eq. 2.1, where now $\mathcal{M}$ is a computational model (no analytic expression, black-box). Here the input is described as a random vector $\boldsymbol{x}$ that has a probability density function (PDF) denoted as $p_{\boldsymbol{X}}$. The computational model converts a specific realization of $\boldsymbol{X} = \boldsymbol{x}$ into an uncertain output $\tilde{y} = \mathcal{M}(\boldsymbol{x})$, which again for the sake of simplicity, is assumed to be an observed realization of a univariate random variable $\tilde{Y} \sim p_{\tilde{Y}}$. The mean value and the variance of $\tilde{Y}$ can be expressed as follows:

$$\mathbb{E}[\tilde{Y}] = \mathbb{E}[\mathcal{M}(\boldsymbol{X})] = \int_{D_x} \mathcal{M}(\boldsymbol{x}) \, p_x(\boldsymbol{x})d\boldsymbol{x} \qquad \text{Eq. 2.11}$$

$$\mathbb{V}[\tilde{Y}] = \mathbb{V}[\mathcal{M}(\boldsymbol{X})] = \mathbb{E}[\mathcal{M}^2(\boldsymbol{X})] - (\mathbb{E}[\mathcal{M}(\boldsymbol{X})])^2 \qquad \text{Eq. 2.12}$$

Since the system's behavior can only be determined in a point-by-point fashion, the integrals in the above equations are analytically intractable. To approximate these integrals, Monte Carlo (MC) methods rely on the law of large numbers [41]. Essentially, the concept behind it, is that the PDF of QoI can be estimated be repeatedly running the simulation with inputs randomly drawn from their corresponding PDF. There are three steps in its implantation [42]:

1. Random sampling: Draw N_{MC} points $\boldsymbol{x}_i$ as independent and identically distributed (i.i.d) samples from $p_{\boldsymbol{X}}$.
2. Numerical experimentation: Evaluate the output for the ith sample $\widetilde{y}_i = \mathcal{M}(\boldsymbol{x}_i)$.
3. Statistical analysis: Compute the statistics on the discrete output points $\widetilde{y}_i$.

Elaborating on the third step, the value of $\widetilde{Y}$ in Eq. 2.11 can be estimated as:

$$\mathbb{E}[\widetilde{Y}] = \frac{1}{N_{MC}} \sum_{i=1}^{N_{MC}} \widetilde{y}_i = \frac{1}{N_{MC}} \sum_{i=1}^{N_{MC}} \mathcal{M}(\boldsymbol{x}_i) \qquad \text{Eq. 2.13}$$

Furthermore, the unbiased estimate of the variance in Eq. 2.12 is computed as:

$$\mathbb{V}[\widetilde{Y}] = \frac{1}{N_{MC} - 1} \left(\sum_{i=1}^{N_{MC}} (\widetilde{y}_i)^2 - N_{MC} \, (\mathbb{E}[\widetilde{Y}])^2 \right) \qquad \text{Eq. 2.14}$$

It is important to mention that MCS can be applied in general for integral estimation even in higher dimensions. This method is known as Monte Carlo integration [43].

2.3.3 Basics of Markov Chains

In order to understand how MCMC methods work, one should familiarize oneself with some basic important concepts regarding Markov Chain theory [44].

State Space

The state space S of a Markov Chain $\{\boldsymbol{X}_t\}$ is the set of all possible realizations (states) of the terms of the chain. For the sake of simplicity in this section the Markov Chain theory is presented on a discrete state space. It is then assumed that:

$$S = \{s_1, \dots, s_m\} \qquad \text{Eq. 2.15}$$

That is, the terms of the chain can take one of m values $s_1, \dots, s_m$. In the following, the notations $i, j \leq m$ will correspond to two different realizations s_i, s_j of the state space.

Markov Property

A sequence of random variables $\{\boldsymbol{X}_1, \boldsymbol{X}_2, \dots, \boldsymbol{X}_t\}$ on a discrete state space S is called a Markov Chain if and only if it satisfies the Markov property, i.e. the conditional probability of $\boldsymbol{X}_{t+1}$ given $\boldsymbol{X}_1, \dots, \boldsymbol{X}_t$ depends only on $\boldsymbol{X}_t$:

Theoretical Background

$$p\big(X_{t+1} = s_j \big| X_t = s_i, \ldots X_1 = s_{i_1}\big) = p\big(X_{t+1} = s_j \big| X_t = s_i\big) \qquad \text{Eq. 2.16}$$

It is also assumed that the Markov Chains in this study are time-homogenous for every $i, j \leq m$, namely:

$$p\big(X_{t+1} = s_j \big| X_t = s_i\big) = p\big(s_j \big| s_i\big) = p_{ij} \in \mathbb{R}^{\Omega \times \Omega} \qquad \text{Eq. 2.17}$$

One should think of the index t as a measure of time. Time-homogeneity proposes that the transition probabilities from one state to another do not depend on time t and thus, there is a constant transition matrix denoted as $\boldsymbol{P} = [p_{ij}]$ as proposed in Eq. 2.17.

It is important to notice that the evolution of a chain is described by the aforementioned transition matrix $\boldsymbol{P}$ and by its occupational distribution at the initial time $t = 1$ (initial distribution): $\boldsymbol{a}^{(1)} = \{a_1^{(1)}, \ldots, a_m^{(1)}\}$, where $a_i^{(1)} = p(X_1 = s_i)$. The initial distribution of a chain is the $1 \times m$ vector of initial probabilities that are assigned to the different states s_i, with $i = 1, \ldots, m$. Considering the transition matrix $\boldsymbol{P}_{ij}$ and the initial probability distribution at time $t = 1$, one can proceed to find the occupational probability distribution of the chain at time $t = 2$ as follows [45]:

$$p\big(X_2 = s_j\big) = \sum_{i=1}^{m} p(X_1 = s_i) \times p(X_2 = s_j | X_1 = s_i) \qquad \text{Eq. 2.18}$$

In other words:

$$a_j^{(2)} = \sum_{i=1}^{m} a_i^{(1)} \times p_{ij} \qquad \text{Eq. 2.19}$$

This can be as well expressed in a matrix form:

$$\boldsymbol{a}^{(2)} = \boldsymbol{a}^{(1)} \times \boldsymbol{P} \qquad \text{Eq. 2.20}$$

One can continue this process, linking each occupational probability distribution to the previous occupational probability distribution. Repeating this process back to the initial state, one can get that:

$$\boldsymbol{a}^{(t)} = \boldsymbol{a}^{(1)} \times \boldsymbol{P}^t = \boldsymbol{a}^{(t-1)} \times \boldsymbol{P} \qquad \text{Eq. 2.21}$$

Irreducible Chain

A discrete Markov chain is said to be irreducible if and only if every state leads to itself and every other state, i.e. if and only if there is a positive probability that for any starting state s_i the chain will reach any other state s_j, including s_i itself, in finite time. In essence when a Markov chain is irreducible all states communicate with each other.

Theoretical Background

Recurrent chain

Suppose a state $s_i \in S$ of a discrete Markov chain. Let V be the total number of visits to the state s_i. The state s_i is called recurrent if and only if:

$$p(V \to \infty | X_1 = s_i) = 1 \qquad \text{Eq. 2.22}$$

In other words, a state s_i is recurrent if and only if the probability that the chain will return to that state in finite time, after started from s_i itself, equals to one. Consequently, a Markov chain is called recurrent if and only if all the elements of its state space are recurrent.

Aperiodic chain

Suppose a recurrent state $s_i \in S$ of a discrete Markov chain. The period of the state s_i is defined as:

$$d_{s_i} = gcd\,\{t > 0 : P_{ii} > 0\} \qquad \text{Eq. 2.23}$$

where gcd is the greatest common denominator. In essence, d_{s_i} is the minimum time the chain takes to return to s_i after starting from s_i itself.

In an irreducible chain all the states have the same period d. A recurrent chain is called aperiodic if and only if the period of the chain equals to one, i.e. $d = 1$.

Stationary distribution

If, for a given transition probability matrix $\boldsymbol{P}$, there is an occupational distribution $\boldsymbol{a}$ such that the distribution of all the terms of the chain is equal to that occupational distribution, then $\boldsymbol{a}$ is called a stationary distribution of the chain. When $\boldsymbol{a}$ is a stationary distribution, then:

$$\boldsymbol{a}^{(t)} = \boldsymbol{a}^{(t-1)} = \boldsymbol{a} \qquad \text{Eq. 2.24}$$

Combining Eq. 2.22 and Eq. 2.24, in order for an occupational distribution a, to be a stationary distribution of a Markov chain, the following must be true:

$$\boldsymbol{a} = \boldsymbol{a}\boldsymbol{P} \qquad \text{Eq. 2.25}$$

Ergodicity and Convergence

When a Markov chain is irreducible and aperiodic, then the Markov chain is ergodic. If a Markov chain is ergodic, then, irrespective of the initial distribution $\boldsymbol{a}^{(1)}$:

$$\lim_{t \to \infty} \boldsymbol{a}^t = \boldsymbol{a} \qquad \text{Eq. 2.26}$$

Where $\boldsymbol{a}$ is the unique stationary distribution of the chain. Basically, even if the initial distribution of the chain is not the stationary distribution, the terms $\boldsymbol{X}_t$ of the sequence become less and less dependent on the initial value $\boldsymbol{X}_1$ as t increases and their distribution converge to the stationary distribution.

Reversibility and Balance Condition

Let $\{X_t\}$ be an irreducible Markov chain with state space S and transition matrix $\boldsymbol{P}$. A probability distribution $\boldsymbol{a}$ on S is said to be reversible for the chain if $\boldsymbol{a}$ and $\boldsymbol{P}$ are in detailed balance, i.e.:

$$a_i p_{ij} = a_j p_{ji} \ for \ all \ s_i, s_j \in S \qquad \text{Eq. 2.27}$$

Consequently, an irreducible Markov chain is said to be reversible if it has a reversible distribution. The Eq. 2.27 is also known as detailed balance condition. The most important outcome of Eq. 2.27 for MCMC methods, is that if probability distribution $\boldsymbol{a}$ on S satisfies the detailed balance condition, then the distribution $\boldsymbol{a}$ is the stationary distribution of the Markov chain [46].

2.3.4 The Metropolis-Hastings (MH) algorithm

Having a general idea about Markov chains and Monte Carlo Simulation, one can perceive MCMC methods as the amalgam of Markov chain philosophy and Monte Carlo sampling. While conventional MC methods generate independent samples, MCMC techniques draw correlated samples, where the next sample is dependent only on the existing previous sample, hence the name Markov Chain. There are a variety of MCMC methods that differ based on the way they construct the Markov chain and the way the generate samples. One of the most common MCMC methods used in Bayesian inference, that is also applied in this study, the Metropolis-Hastings (MH) algorithm.

The MH algorithm constructs an ergodic Markov chain such that its stationary distribution equals the posterior distribution of the Bayesian problem. Based on the section 2.2, let $\pi(\boldsymbol{x})$ be the prior and $p(\boldsymbol{x}|\boldsymbol{y})$ be the posterior density of some QoI $\boldsymbol{x}$. A Markov chain with stationary distribution $p(\boldsymbol{x}|\boldsymbol{y})$ is generated by initializing at $\boldsymbol{x}^{(0)}$ from the prior density, and then repetitively proceeding as follows. Given a state $\boldsymbol{x}^{(t)}$ that the Markov chain has taken on in some iteration t, in the following iteration a candidate state $\boldsymbol{x}^{(*)}$ is randomly sampled from a proposal distribution $q(\boldsymbol{x}^{(*)}|\boldsymbol{x}^{(t)})$. In the MH correction step the proposed state is approved as the new state $\boldsymbol{x}^{(t+1)} = \boldsymbol{x}^{(*)}$ of the Markov chain with probability:

$$a\left(\boldsymbol{x}^{(*)}, \boldsymbol{x}^{(t)}\right) = min\left(1, \frac{p\left(\boldsymbol{x}^{(*)}|\boldsymbol{y}\right)q(\boldsymbol{x}^{(t)}|\boldsymbol{x}^{(*)})}{p\left(\boldsymbol{x}^{(t)}|\boldsymbol{y}\right)q(\boldsymbol{x}^{(*)}|\boldsymbol{x}^{(t)})}\right) \qquad \text{Eq. 2.28}$$

Otherwise, the proposal will be rejected, i.e. the Markov chain remains in its state $\boldsymbol{x}^{(t+1)} = \boldsymbol{x}^{(t)}$ of the preceding iteration. In practice, the acceptance process is performed by sampling a random number u from a uniform distribution in the interval [0,1]. The proposed state is accepted if $u < a\left(\boldsymbol{x}^{(*)}, \boldsymbol{x}^{(t)}\right)$, otherwise it is rejected. It is important to note that due to the MH acceptance probability Eq. 2.28, the algorithm calls for the computation of posterior ratios only. Thus, the model evidence term of Eq. 2.7 can be dropped and only the unnormalized posterior density has to be evaluated. Another key point that needs to be outlined is that the MH algorithm achieves to sample from the posterior because the acceptance probability Eq. 2.28 is equivalent to the

posterior distribution satisfying the detailed balance condition in Eq. 2.27, which results to the posterior being the stationary distribution of the Markov chain [46].

One way to simplify the aforementioned algorithm is to choose a symmetric proposal distribution, namely a proposal distribution that satisfies the following condition: $q(x_a|x_b) = q(x_b|x_a)$ for all x_a, x_b and t. Then Eq. 2.28 becomes simply:

$$a\left(\boldsymbol{x}^{(*)}, \boldsymbol{x}^{(t)}\right) = min\left(1, \frac{p\left(\boldsymbol{x}^{(*)}|\boldsymbol{y}\right)}{p\left(\boldsymbol{x}^{(t)}|\boldsymbol{y}\right)}\right) \qquad \text{Eq. 2.29}$$

In that case the algorithm is called just Metropolis algorithm. A common symmetric proposal distribution that is chosen is a normal Gaussian distribution that is centered around the current state $\boldsymbol{x}^{(t)}$, namely $\boldsymbol{x}^{(*)} \sim \mathcal{N}(\boldsymbol{x}^{(*)}; \boldsymbol{x}^{(t)}, \Sigma_x)$. This process is known as Random Walk Metropolis sampling [47]. The algorithm that is employed in the present study is a Random Walk Metropolis sampling algorithm.

At this moment it is important to point out that an MCMC algorithm is rarely initialized from its stationary distribution. This fact raises the concern that these initial values might bias the results even if the process reaches stationarity later on. To compensate for this, a burn-in period is often implemented, i.e. the first T samples being discarded, with T being chosen to be large enough so that the chain has reached its stationary regime by its time. In Figure 2.3 an indicative trace plot is illustrated. A trace plot is a graph of the sampled parameter values as a function of the step iterations. In essence, a trace plot presents the chain trajectory. On the trace plot of Figure 2.3 one can clearly see the burn-in period and how the chain values in this period do not belong to the stationary distribution.
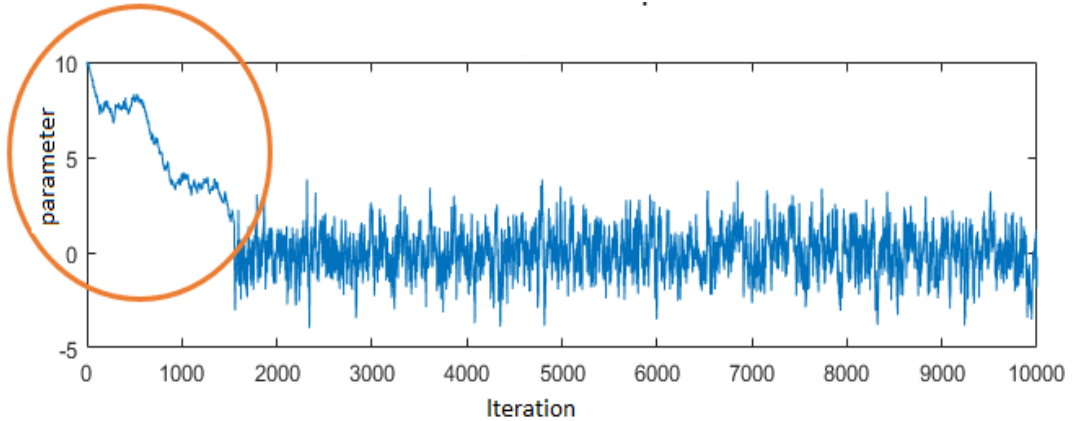
Figure 2.3: Trace plot of a parameter of interest, where the circled region represents the burn-in period. (Source: [48]).

2.3.5 Autocorrelation

As mentioned before, in MCMC algorithms each subsequent sample is drawn using the current sample, resulting typically in the generation of correlated samples. This can be

an important problem since correlated samples can result in biased estimation of the posterior characteristics. However, two samples x_t and x_{t+n} become asymptotic independent as the number n increases, namely the correlation between those samples decays as the number n increases. One can then proceed to assess the independency of the MCMC samples by calculating the effective sample size [49], i.e. the sample size that corresponds to fully random independent samples. In the present study, the effective sample size will not be calculated, but the samples' correlation will be visually evaluated with trace plots and autocorrelation function graphs (ACF graphs).

The ACF graph, also known as correlogram, shows the correlation between samples as a function of the values of n (known as lags). It represents a correlation coefficient and is calculated as follows. Consider the MCMC samples $\{x_t\}$ where $t = 1, \dots, T$ the number of iterations. The mean value of those samples is given by:

$$\overline{x} = \frac{1}{t} \sum_{t=1}^{T} x_t \qquad \text{Eq. 2.30}$$

The autocovariance function at lag n, for $n \geq 0$, of the sequence is defined by:

$$C_n = \frac{1}{t} \sum_{i=1}^{t-n} (x_i - \overline{x})(x_{i+n} - \overline{x}) \qquad \text{Eq. 2.31}$$

Then the ACF at lag n, for $n \geq 0$, of the sequence is defined by:

$$r_n = \frac{C_n}{C_0} \qquad \text{Eq. 2.32}$$

An indicative correlogram is shown in Figure 2.4, where the autocorrelation is large at short lags, but it goes quickly to zero as it should be in a successful MCMC process.
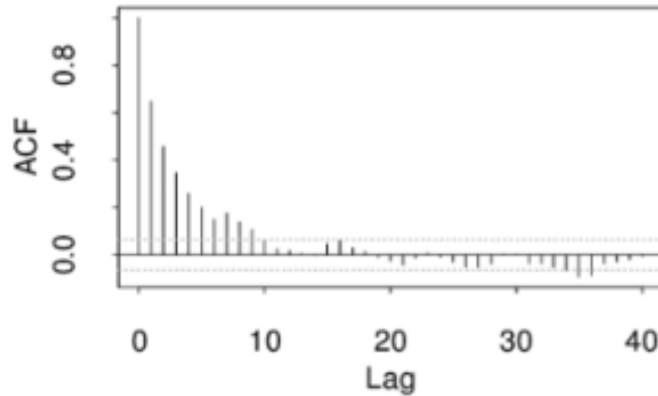
Figure 2.4: Indicative ACF graph (correlogram). (Source [50]).

At this moment it is important to point out that the covariance matrix Σ_x of the proposal distribution determines the "stepsizes" of the algorithm, hence being a key aspect to the samples' autocorrelation. Either choosing too large or too small variance for the

proposal distribution will give highly correlated samples. This is illustrated in Figure 2.5.
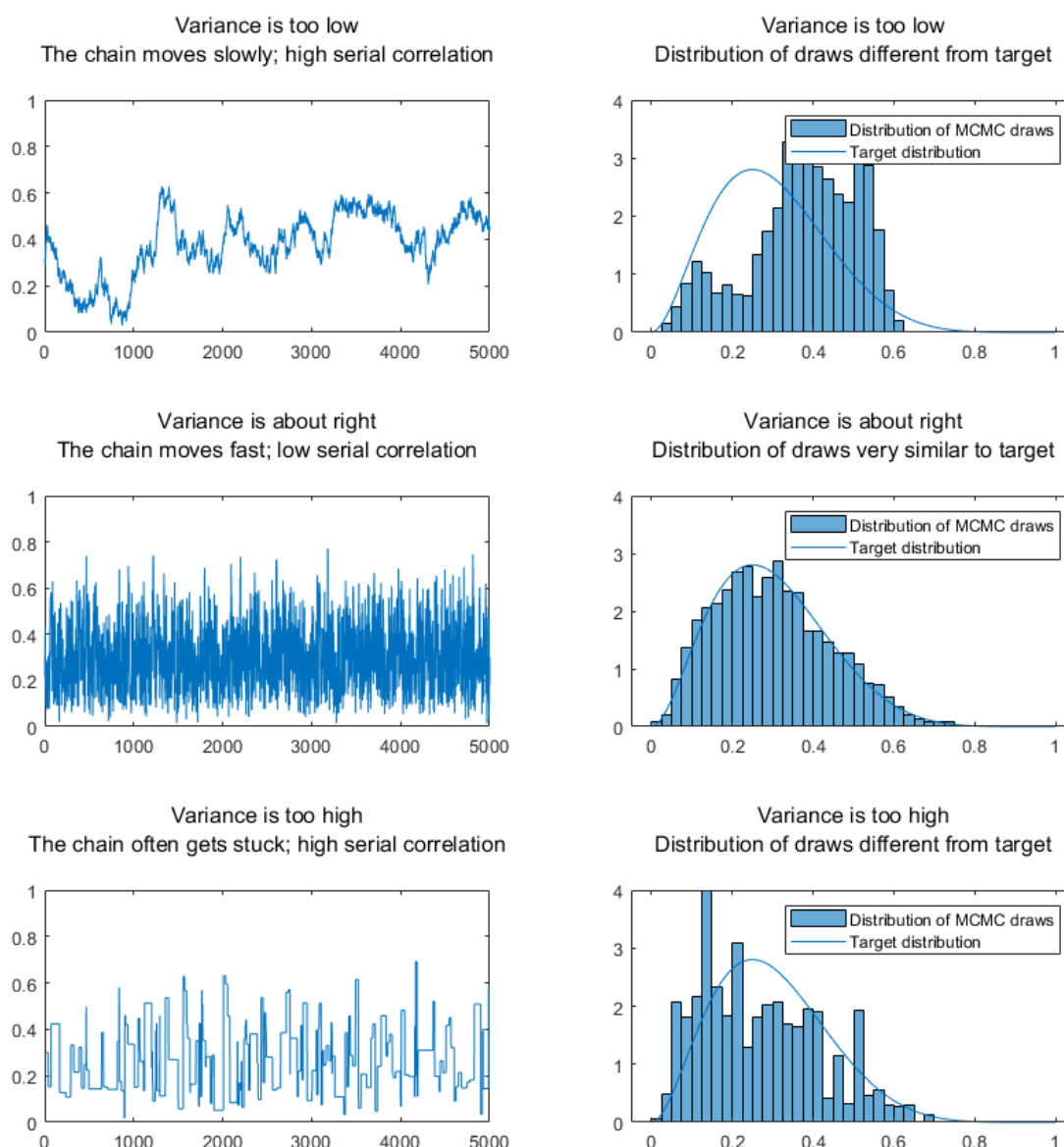
Figure 2.5: Chain behavior illustration (trace plots and PDF histograms) for different values of variance of the proposal distribution. (Source [48]).

The situations presented in Figure 2.5 are also connected to the acceptance rate of the chain. In the first line the algorithm has a very high acceptance rate, making the chain move extremely slowly, and though convergence may be achieved, it will happen after an inefficient number of iterations. On the other hand, in the third line the acceptance rate is very low, and the chain gets stuck to some locations needing hundreds of iterations to take just one step to a new location. For the MH algorithm the optimal range of the acceptance rate is between 10% to 60%.

2.3.6 Convergence Diagnostics

One major issue when dealing with MCMC methodologies is to assess whether the chain has converged to the stationary posterior distribution and to the asymptotic

independence. These issues are monitored with a variety of diagnostic tools [49], however in this study the convergence and sampling behavior will be evaluated visually by examining trace plots after running multiple chains.

Figure 2.6 illustrates two of the challenges of monitoring convergence of MCMC simulations. The left graph shows two sequences for the same QoI but with different initial state, each of which looks fine on its own (and indeed, when looked at separately would be thought to have achieved convergence), but the juxtaposition makes it clear that they have not converged to a common distribution. This graph illustrates that, to achieve convergence, the sequences must be mixed. The right graph in Figure 2.6 shows two chains that have mixed, in the sense that they have traced out a common distribution, but they do not appear to have converged to a stationary distribution overall. This graph illustrates that, to achieve convergence each individual sequence must reach stationarity.
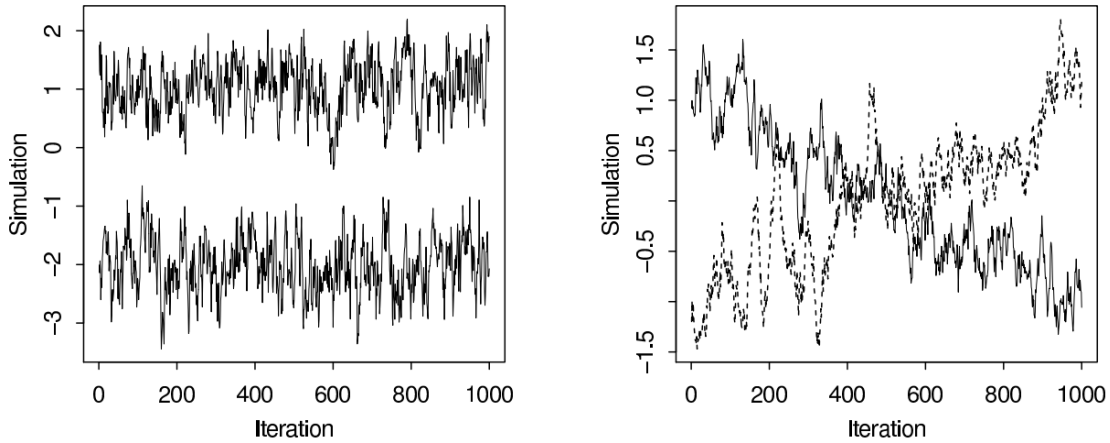
Figure 2.6: Examples of two challenges in assessing convergence of MCMC algorithms. (Source [51]).

Based on the aforementioned the diagnosis of convergence is being performed by evaluating mixing and stationarity with the following simple approach. One first creates a few chains (at least three) each of which has a different initial state. It is important to note that the burn in period on these sequences must be discarded. Then, each created chain is split in half, and it is checked if all the resulting half-sequences have mixed. This simultaneously tests mixing (if all the chains have mixed well, the separate parts of the chains should also mix) and stationarity (if the first and second half of each sequence is traversing the same distribution).

2.4 Surrogate Modeling

2.4.1 General

Due to the iterative nature of the MCMC methods in Bayesian inference, these methods are tied with high computational cost. This aspect of MCMC makes the use of surrogate modeling an appealing approach to gain computational efficiency. Surrogate modeling, also known as metamodeling, refers to the practice of constructing an approximate, yet less expensive, representation of the input-output relationship of a complex physical

process, like the one described in section 2.1.2. The produced model can then be evaluated at negligible cost to predict the outputs for a new set of inputs that exist within the initial observation domain [42]. The rise of Machine Learning (ML) and data-driven modeling [52] has made the concept of surrogate modeling even more viable, with potential applications in many areas, including SHM [53], material science [54] and many other.

In general, a surrogate model does not maintain any virtual representation of the exact nature of the physical system of interest, but rather approximates its complex behavior exclusively based on a finite set of simulation data (support points) without requiring problem-specific knowledge (black-box model). Therefore, operational (e.g., loads) or state (e.g., damage features) information about the structure is integrated within the constructed surrogate model, allowing immediate access to predictions when a batch of input data is obtained from the system. As the approximate function is created based on the information carried by the support points, it is essential to generate informative pairs of data samples. To this end, the employed physics-based model $\mathcal{M}$ is typically exploited within a simulation framework, which ends up with a list of data points, known as training data, expressed as:

$$\{x_j; \tilde{y}_j\} \qquad \text{Eq. 2.33}$$

Where x_j is the jth input vector from the sampling plan, and $\tilde{y}_j$ includes the corresponding outputs from evaluating the model $\mathcal{M}$, i.e., $\tilde{y} = \mathcal{M}(x)$. The learning stage of the surrogate models is usually undertaken offline, whereas only the evaluation of model prediction occurs during the online stage allowing for future re-use and re-production. In case of physical changes to the system, however, the surrogate model needs to be retrained. The surrogate predictions are denoted as $\hat{y}$, the corresponding surrogated model is denoted as $\widehat{\mathcal{M}}$, and its formulation is shown in Eq. 2.34:

$$\tilde{y}_j = \hat{y} + \eta_j = \widehat{\mathcal{M}}(x_j) + \eta_j \qquad \text{Eq. 2.34}$$

Where η_j is the error (residual) that describes the discrepancy between real observations $\tilde{y}_j$ and approximations $\widehat{\mathcal{M}}(x_j)$. Depending on the degree of non-linearity of the mapping function a different modeling approach may be used. Among the most prevalent approximation approaches are linear/polynomial regression, Gaussian processes, neural networks and support vector machines to name a few. In the present work polynomial regression and support vector machines are employed on two different occasions in order to construct a surrogate that learns a mapping between the input parameters and the output response.

2.4.2 Polynomial Regression

In polynomial regression the relationship between the input vector x_j and the output $\tilde{y}_j$ is modelled as an r-th degree polynomial in x_j. A nonlinear function is fitted to the data points, namely:

$$\tilde{y}_j = b_0 + b_1 x_j + b_2 x_j{}^2 + \cdots + b_r x_j{}^r + \eta_j \qquad \text{Eq. 2.35}$$

In order to estimate the polynomial coefficients $b_0, b_1, \ldots, b_r$ the least square method is applied [55]. According to the method, the estimation of the polynomial coefficients requires the minimization of the sum of squared errors (SSE), i.e.:

$$SSE = \sum_{j=1}^{J} \eta_j{}^2 = \sum_{j=1}^{J} (\tilde{y}_j - b_0 - b_1 x_j - b_2 x_j{}^2 - \cdots - b_r x_j{}^r)^2 \qquad \text{Eq. 2.36}$$

Where J is the total number of training data. To proceed to the minimization, one needs to differentiate SSE in turn with respect to $b_0, b_1, \ldots, b_r$ and equate to zero. Thus, a set of $r + 1$ normal equations will be generated.

$$Jb_0 + b_1 \sum_{j=1}^{J} x_j + b_2 \sum_{j=1}^{J} x_j{}^2 + \cdots + b_r \sum_{j=1}^{J} x_j{}^r = \sum_{j=1}^{J} y_j$$

$$b_0 \sum_{j=1}^{J} x_j + b_1 \sum_{j=1}^{J} x_j{}^2 + b_2 \sum_{j=1}^{J} x_j{}^3 + \cdots + b_r \sum_{j=1}^{J} x_j{}^{r+1} = \sum_{j=1}^{J} x_j y_j$$

$$\vdots \qquad \vdots \qquad \vdots \qquad \vdots \qquad \vdots \qquad \vdots \qquad \text{Eq. 2.37}$$

$$b_0 \sum_{j=1}^{J} x_j{}^r + b_1 \sum_{j=1}^{J} x_j{}^{r+1} + b_2 \sum_{j=1}^{J} x_j{}^{r+2} + \cdots + b_r \sum_{j=1}^{J} x_j{}^{2r} = \sum_{j=1}^{J} x_j{}^r y_j$$

These equations can then be solved for $b_0, b_1, \ldots, b_r$ by any appropriate analytic method for solving systems of equations, however most of times statistical software is used to obtain numerical solutions.

2.4.3 Support Vector (SV) Regression

When the complexity, non-linearity and the dimensions of an engineering problem increase, simple linear/polynomial methods tend to make inaccurate predictions, and more advanced regression methods need to be employed. Support vector machine (SVM) analysis is a popular machine learning tool for classification and regression [56]. It is considered a nonparametric technique because it relies on Kernel functions.

Suppose one is given the training data $\{x_j; \tilde{y}_j\}$. In ε-SV regression, the goal is to find a function $f(x)$ that has at most ε deviation from the actually obtained targets $\tilde{y}$ for all the training data and at the same time is as flat as possible. In other words, the errors are not important as long as they are less than ε, but any deviation larger that this will not be accepted. This function that predicts the values $\hat{y}$ is expressed as follows:

$$\hat{y} = \widehat{\mathcal{M}}(x) = w^T K(x_j, x) + b \qquad \text{Eq. 2.38}$$

Where w is the weight vector and b is an offset. The non-linear mapping function $K(x_j, x)$ is the Kernel function [57]. Using input data mapping in a high-dimensional space the Kernel function changes the nonlinear regression problem into a linear

regression problem in the higher dimension. In the present study a Gaussian Kernel function is employed i.e., for two points x_j, x_i:

$$K(x_j, x_i) = exp\left(-\|x_j - x_i\|^2\right)$$

Eq. 2.39

In order to achieve flatness, one needs to seek small w. One way to ensure this is to minimize the norm $\|w\|^2$. This can be formulated as a convex optimization problem. However, the existence of a function $\widehat{\mathcal{M}}(x)$ that approximates all pairs $\{x_j; \tilde{y}_j\}$ with ε precision assumes that the optimization problem is feasible. Most of the times this is not the case, and many times it is useful to allow for some errors to avoid overfitting [58]. To achieve that, the slack variables ξ_j and $\xi_j{}^*$ are introduced. These variables allow regression errors to exist up to the value ξ_j and $\xi_j{}^*$, yet still satisfying the required conditions (see soft margin concept [59]). Consequently, one can write this convex optimization problem as follows:

$$Minimize \ \frac{1}{2}\|w\|^2 + C\sum_{j=1}^{J}(\xi_j + \xi_j{}^*)$$

$$Subject\ to \begin{cases} \tilde{y} - w^T K(x_j, x) - b \le \varepsilon + \xi_j \\ w^T K(x_j, x) + b - \tilde{y} \le \varepsilon + \xi_j{}^* \\ \xi_j, \xi_j{}^* \ge 0 \end{cases}$$

Eq. 2.40

The constant $C > 0$ determines the trade-off between the flatness of $\widehat{\mathcal{M}}(x)$ and the amount up to which the deviations larger than ε are tolerated. This corresponds to dealing with a so called ε-sensitive loss function described by:

$$|\xi|_\varepsilon = \begin{cases} 0 & if\ |\xi| \le \varepsilon \\ |\xi| \le \varepsilon & otherwise \end{cases}$$

Eq. 2.41

The optimization described above is computationally simpler to solve in its Lagrange dual formulation. The solution to the dual problem provides a lower bound to the solution of the primal (minimization) problem. The optimal values of the primal and dual problems does not need to be equal, and the difference is called the "duality gap." But when the problem is convex and satisfies a constraint qualification condition, the value of the optimal solution to the primal problem is given by the solution of the dual problem. One can obtain the dual formula by introducing non-negative multipliers a_j and $a_j{}^*$ for each observation. Then the following quantity must be minimized:

$$L(a) = \frac{1}{2}\sum_{j=1}^{J}\sum_{i=1}^{J}(a_j - a_j{}^*)(a_i - a_i{}^*)K(x_j, x_i) + \varepsilon\sum_{j=1}^{J}(a_j + a_j{}^*)$$
$$+ \sum_{j=1}^{J} y_j(a_j{}^* - a_j)$$

Eq. 2.42

Subject to the constrains:

$$\sum_{j=1}^{J} \left(a_j - a_j^* \right) = 0 \quad , \qquad a_j, a_j^* \in [0, C] \qquad \text{Eq. 2.43}$$

Furthermore, the offset parameter b, is computed by exploited the Karush-Kuhn-Tucker (KKT) conditions which state that at the point of the solution the product between the dual variables and the constrains has to vanish [57].

After estimating all the required parameters, one can proceed to predictions for new values $\boldsymbol{x}$, based on the following function:

$$\hat{y} = \widehat{\mathcal{M}}(\boldsymbol{x}) = \sum_{j=1}^{J} \left(a_j - a_j^* \right) K\left(\boldsymbol{x_j}, \boldsymbol{x} \right) + b \qquad \text{Eq. 2.44}$$

2.5 Fundamentals of Finite Element Analysis (FEA)

The recent advances in computational resources have allowed the development of high-fidelity models to address the increased complexity of modern engineering systems. The present study makes use of such a model to generate a sufficient amount of structural response data (i.e., strain measurements) that is necessary for training the aforementioned employed surrogate models. For this formulation, the Finite Element Method (FEM) was employed, which is a widely used numerical technique for the simulation of complex physical phenomena. It was deemed appropriate to include some basic theoretical elements of FEM to accompany the present study.

2.5.1 Basic Principles of the FEM

The Finite Element Method (FEM) is essentially a simulation of the continuum as a series of fundamental elements interconnected at a finite number of points referred to as nodes. As far as frames are concerned, which consist of a number of beams connected to each other at specific points, FE modeling is very intuitive since physical boundaries and connection points between members already exists (visual example presented in Figure 2.7). Regarding continuous structures such as the hull of a ship, or other plate like structures, where no physical discretization is existent, the entire domain needs to be virtually separated into smaller constituting elements (visual example presented in Figure 2.8). The elements can be one-dimensional (beams), two-dimensional (triangular or rectangular) or even three-dimensional (tetrahedrals etc). The nodes are usually positioned on their corners or edges but can even be in the inside of the elements depending on the architecture of the element.
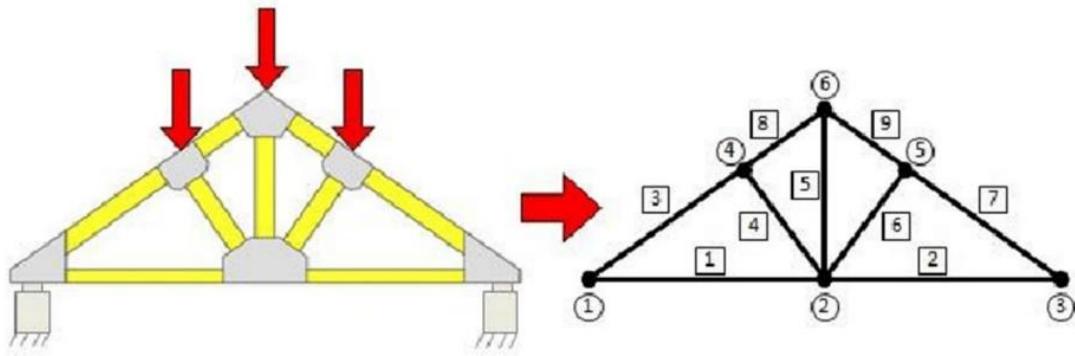
Figure 2.7: Example of discretization of a 2D structural frame into a FE model consisting of nine elements and six nodes. (Source: [60]).
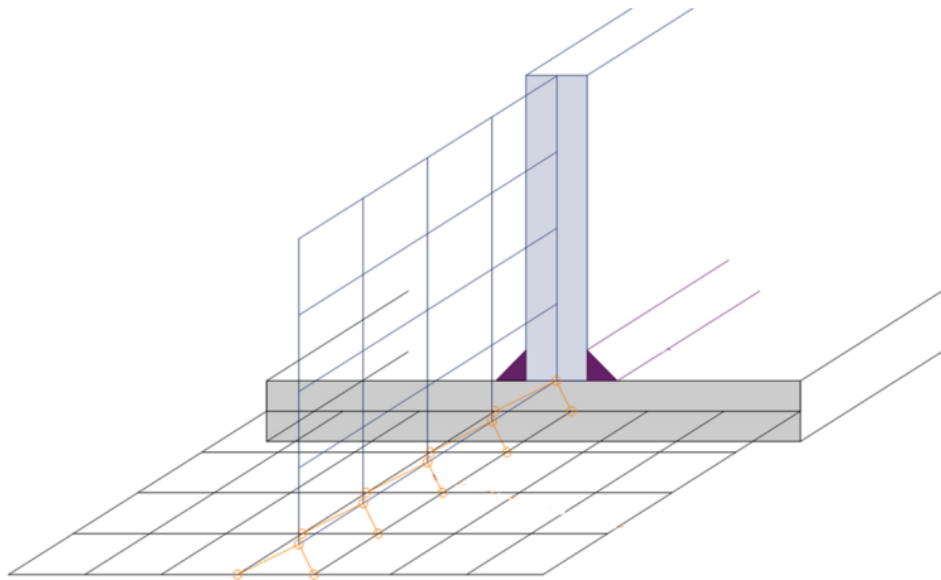
Figure 2.8: Example of FE modeling of a T joint between two thin-walled plates. (Source: [61]).

The continuous domain is simulated as a series of discrete variables or degrees of freedom, usually defined as the nodal displacements and optionally their derivatives as well. Displacements inside each element must be compatible with the nodal displacements and are directly dependent on the corresponding values at the nodes. As a result, the structural response is approximated by calculating all nodal displacements. The continuous problem is therefore transformed into a discrete one. Acquiring the structural response comes down to forming the equilibrium equations at the nodes and then solving the resulting system with respect to nodal displacements.

To achieve an accurate solution, there are some conditions that need to be satisfied. Namely, conditions of equilibrium as well as geometrical continuity inside the elements and along their edges. It is interesting to note that a collection of elements connected only at their nodes is not a direct analogous of the continuum, as displacement continuity is only explicitly imposed at the nodes, thus gaps or overlaps between members can occur following this modelling approach (visual example presented in

Figure 2.9). Of course, it should always be taken into consideration that the FEM is meant to approximate reality and is not expected to produce exact results.
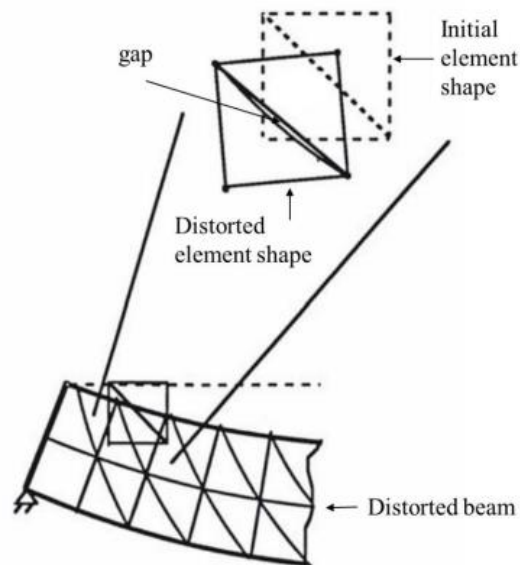
Figure 2.9: Example of gap forming between the edges of triangular elements in the distorted state. Case of modeling a beam cantilever with triangular shell elements. (Source: [62]).

However, with the implementation of several techmiques, this inherent error can be mitigated to an acceptable level for each application. The simplest approach to reduce inaccuracies in FE modelling is by using an increased number of smaller elements. Increased accuracy by increasing the fidelity of the model comes at the cost of increased need of computational power and time requirements.

Nonetheless, there are more sophisticated methods to increase accuracy. More specifically, each element is characterized by its shape function. The shape function takes the nodal values of a field quantity (such as the displacement) and projects it throughout the entire elemental domain. Appropriate design of the shape function can guarantee equilibrium and geometrical continuity inside the elements and along their boundaries while only enforced at the nodes. Several element types and shape functions are available in the literature and are included in commercial FEA software, each optimized for a specific type of application. It is clear that careful selection of the element architecture is important in achieving greater solution accuracy.

In FEM, equilibrium is not necessarily satisfied at every location of the continuous domain. Regardless, there are two conditions that must always be satisfied. In particular these are:

a) Equilibrium of forces (external and internal) on every node.
b) Equilibrium of nodal forces of every element.

The aforementioned conditions are visually summarized in Figure 2.10.
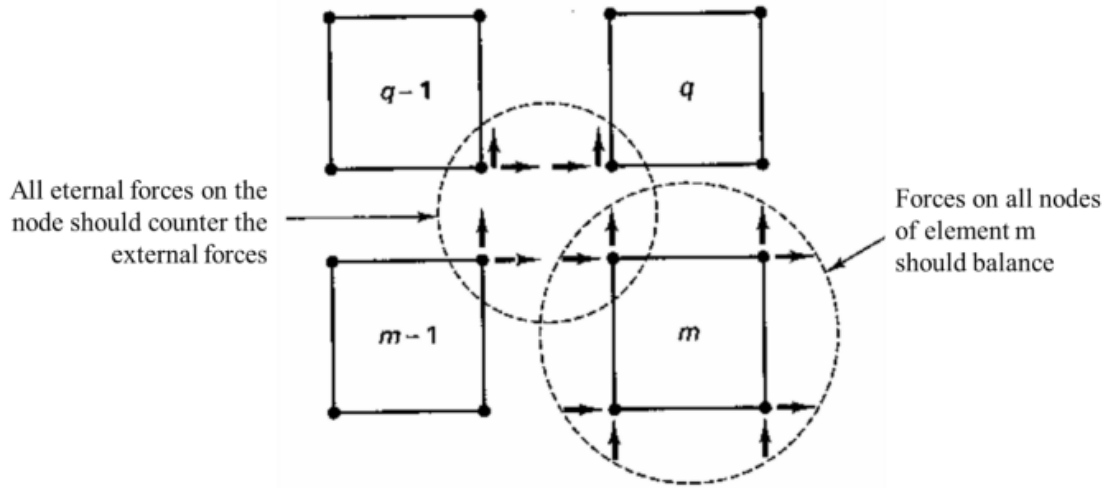
Figure 2.10: Visual explanation of elemental equilibrium and nodal equilibrium on an indicative FE mesh. (Source: [62]).

The generalized form of the system of equilibrium equations of a FE model can be summarized in:

$$\{F\} = \{K\} \times \{U\} \qquad \text{Eq. 2.45}$$

where $\{F\}$ is the vector that contains all external force effects expressed as equivalent forces on every node. $\{K\}$ is the global stiffness matrix of the system and $\{U\}$ is the column vector containing all nodal displacements, the dependent variables or degrees of freedom (DOFs) of the system.

The global stiffness matrix ($\{K\}$) is derived as a direct superposition of the stiffness matrix of every element ($\{K\}^m$).

$$\{K\} = \sum_m \{K\}^m \qquad \text{Eq. 2.46}$$

Commonly, the stiffness matrix of an element will be available in the literature regarding a specific element type. In general, the elemental stiffness matrix is expressed in terms of a local, on-element coordinate system. Before superimposing, each member stiffness matrix is expressed in terms of the selected global coordinates system and projected to the dimensions of the global stiffness matrix. Namely, a transformation to the coordinate system that is defined for the entire composite model is required. This global reference system does not coincide with the local systems of every element for most complex structures. The required transformation is executed with the use of a transformation matrix $\{T\}$, which incorporates all necessary rotational conversions to reposition the reference system of the initial matrix. This is described in mathematical terms in Eq. 2.47.

$$\{K\}^m = \{T\}^T \{\widehat{K}\}\{T\} \qquad \text{Eq. 2.47}$$

The ^ notation is introduced to distinguish the matrixes which refer to the local coordinate system from their counterparts, those referring to the global coordinate system of the model.

Once the elemental stiffness matrices ($\{K\}^m$) have been formulated and expressed in the global coordinate system, the stiffness matrix of the entire model can be constructed as shown in Eq. 2.46.

The subsequent step in establishing a FE model is to appropriately define any external loading and boundary conditions. The first are incorporated in $\{F\}$ matrix, as introduced earlier. In the discretised reality of FEA, where all external forces should be applied on nodes, it is important that any concentrated point loads coincide with a node in the model. Consequently, operational conditions should be taken into account when discretizing the model. It is made obvious that any distributed pressure loads are required to be discretized to equivalent point loads on node locations.

As far as boundary conditions are concerned, these can be integrated as constraints of DOF in the displacement vector $\{U\}$. Superficially, this procedure might be regarded as easy as setting some variable to a fixed value because of the way supports are modelled in classical mechanics theory. Nonetheless, when accuracy is desired, the application of idealized theoretical boundary conditions may not be acceptable. As a result, detailed modelling of the supports and boundary interactions may be required. For this matter, the analyst is expected to have ample theoretical knowledge and intuition regarding the problem at hand.

It is important to keep in mind that in modern FEA environments most of the heavy mathematical workload has been automated and assigned to computers. Nevertheless, appropriate modelling of the problem, as well as evaluation and interpretation of the results still require human expertise and should not be adopted without judgement. Often, results from FEA are compared directly to results acquired from analytical solutions or experimental measurements where applicable. This practice ensures validity of the modelling and in case of significant deviations indicates the need for potential adjustments.

2.5.2 FE Modeling of Thin-walled Structures

The general procedure of structural analysis using the FEM has been introduced in the previous subsection. In the present work, a thin-walled plate structure falls in the scope of analysis. It was considered appropriate to discuss some more details regarding modelling thin-walled structures in FEA.

Thin-walled structures are defined as these structures in which thickness is of much smaller magnitude than the rest of the dimensions. The prevalence of thin-walled components and structures in every domain is justified by their optimized nature in terms of material and weight economy. With clever geometrical modifications (e.g. stiffeners, corrugation) the desired stiffness and stability are achieved with significantly reduced thickness, resulting in less structure weight and less material requirements. Such thin-walled arrangements are common in marine constructions and include plates,

bulkheads, stiffened panels, or even the entire hull, often regarded as a thin-walled hollow girder to study its response in global bending and twisting.

Thin-walled structures can be modeled using rectangular, flat, shell-type elements. Shell geometries are fully defined by their mid-surface and thickness. In general, a thin-walled arrangements will be subjected to bending as well as in plane stresses. Assuming operation in the range of small deformations, the deformations due to bending and due to the plane stress conditions can be considered independent [63]. In this regard, the shell element can be derived by superimposing a plane stress element with a bending element [62] as seen in Figure 2.11.
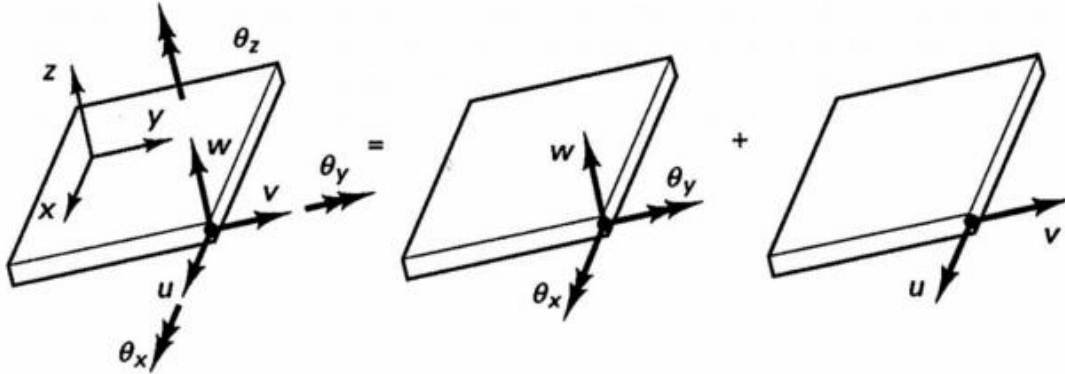
Figure 2.11: Modeling of a flat "shell" element by superimposing a "bending" and a "plane stress" element. (Source: [62]).

This principle allows to simplify the formulation of the shell element, as its stiffness matrix can be produced by appropriately adding the stiffness matrices of its other two components. The stiffness matrices $\{\widehat{K_B}\}$ and $\{\widehat{K_P}\}$ of the bending and plane stress elements accordingly are available in the literature [62].

The resulting stiffness matrix for the shell element can be produced as follows:

$$\{\widehat{K_B}\} = \begin{bmatrix} \{\widehat{K_B}\} & \{0\} \\ \{0\} & \{\widehat{K_P}\} \end{bmatrix}$$

Eq. 2.48

Since the bending model has three DOFs per node and a total of 4 nodes, the accompanying stiffness matrix will be 12×12 sized. Equivalently, for the plane stress element with two DOFs per node, the stiffness matrix will be 8×8 sized. Consequently, the stiffness matrix of the resulting shell element, as per the formulation of Eq. 2.48, will be a 20×20 matrix. In the aforementioned equation $\{0\}$ symbolizes appropriately shaped zero matrices.

In order to integrate the local, elemental stiffness matrix $\{\widehat{K_B}\}$ of a shell element to the global stiffness matrix of an entire model, as mentioned in a previous paragraph, a transformation to the global coordinate system is required. Similarly, the transformation can be written as follows:

$$\{K\}^m = \{T\}^T\{\widehat{K_S}\}\{T\}$$

Eq. 2.49

Consequently, to model a thin-walled structure the discretization of its geometry must be decided, taking into account the loading conditions and any relevant constraints. The global stiffness matrix describing the entire model can then be constructed as per Eq. 2.46.

Following the methodology of the previous subsection, the loads should be discretized and incorporated in the forces vector. Then the boundary conditions should be modelled appropriately and expressed in terms of constraints of DOF in the displacement vector. Once the above are completed, getting the response of the structure comes down to solving the system of Eq. 2.45.

3 Problem Definition

This section aims to offer a detailed description of the key parameters defining the reference problem studied in this work. Firstly, the problem geometry is described followed by the definition of the variable operational loads and damage states. Onwards, the proposed virtual sensor topologies are presented. Finally, details of the FE modelling, the source of the required data for this exploratory analysis, are discussed. It should be noted that, because this study is an expansion of the work by Katsoudas [17], the problem definition sections in both studies show many similarities.

3.1 Idealized Plate Domain

A ship is a complex structure and that can pose a serious modeling and computational challenge for numerical simulations. However, this complex design consists of simple structural entities such as plates and beams. These structural elements have been studied in detail in the past century and thus there is plenty of knowledge built around the behavior and modeling of such geometries. A SHM system can also be focused on individual structural components ensuring that if each component is safe the structural integrity as a whole is guaranteed.

The most common structural element on a ship is the stiffened panel, a typical arrangement of which is pictured in Figure 3.1. Albeit, for the purposes of this theoretical study, the geometrical domain was decided to be a rectangular (square) $a_0 \times a_0$-sized plate with a thickness of 1% its other principal dimensions. For simplification purposes, the value of a_0 is set to one meter.
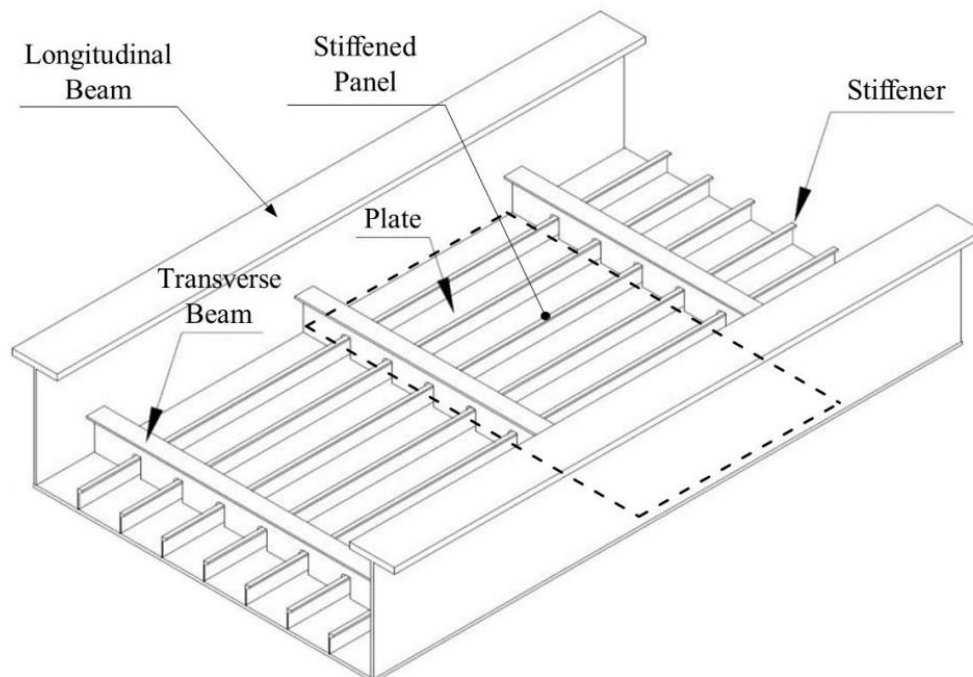

Figure 3.1: Typical structural arrangement of a ship's hull bottom. (Source: [64]).

3.2 Loading Conditions

The aforementioned plate was subjected to two different operational conditions. First, the plate was considered to be subjected to a variable operational load. The load magnitude and its center location were modeled as random variables. The pressure profile is selected to be represented by the product of exponents of the quadric relation of the centroid of a bell-shaped curve. The mathematical expression of this non-uniform pressure profile is shown in Eq. 3.1.

$$q(x, y; Q_0, \bar{X}, \bar{Y}) = Q_0 exp \left(-\frac{1}{2} \left(\frac{x - \bar{X}}{s} \right)^2 \right) \left(-\frac{1}{2} \left(\frac{y - \bar{Y}}{s} \right)^2 \right) \qquad \text{Eq. 3.1}$$

In the above, s is a deterministic shape parameter, x, y are deterministic variables representing coordinates on the plate plane relative to its centers as depicted in Figure 3.2. The variability of the load is controlled through the peak amplitude Q_0 at the location of the peak of the load at $(\bar{X}, \bar{Y})$. These quantities are considered to be independent continuous random variables following a normal distribution, i.e., $Q_0 \sim \mathcal{N}(q_0; \mu_{Q_0}, \sigma_{Q_0})$, $\bar{X} \sim \mathcal{N}(\bar{x}, \mu_{\bar{X}}, \sigma_{\bar{X}})$, $\bar{Y} \sim \mathcal{N}(\bar{y}, \mu_{\bar{Y}}, \sigma_{\bar{Y}})$. The particulars of each distribution were appropriately selected in order to achieve specific behavior of the load. The parameters of the load amplitude μ_{Q_0}, σ_{Q_0} were selected such that the plate remains within the elastic regime and the load is distributed between zero and a maximum value. Furthermore, it was decided that the load random location would be symmetrically distributed around the center of the plate $(0,0)$, which leads to $\mu_{\bar{X}} = \mu_{\bar{Y}} = 0$. An indicative three-dimensional plot of the load profile around an arbitrarily selected center is presented in Figure 3.3.

The equation defining the load yields a symmetrical around its center, bell-shaped surface that represents the load magnitude at each point. The surface extends to infinity along both axes of the plate plane. Due to the fact that the distribution is a product of exponents, the amplitude of the load degrades to zero in an asymptotic way within a relatively short distance from its center. Thus, the significant part of the distribution, where non-zero amplitude is observed, is considered to be bound within a diameter extending six times the value of s around the center. The value of the s parameter is set to be equal to $a_0/12$. Consequently, the distribution of the load is constrained within a circular like area with a diameter of $a_0/2$, denoted with the red concentric circles in Figure 3.2.

In order to fit the significant part of the load within the structural domain, its peak coordinates $(\bar{X}, \bar{Y})$ had to be constrained within specified boundaries. Assuming that the range of $(-3\sigma, +3\sigma)$ around the mean of each coordinate is equal to the range $(-1/4\,\alpha_0, +1/4\,\alpha_0)$ on the plate, then the defined significant part of the load will fit completely within the structural domain with a probability of 99.46%. The latter is the product of the 99.73% probability of each independent coordinate value to be sampled within the specified range of 6σ, according to the known theory for random variables

following the normal distribution. Hence, the standard deviation of each coordinate was selected as $\sigma_{\bar{X}} = \sigma_{\bar{Y}} = a_0/12$.
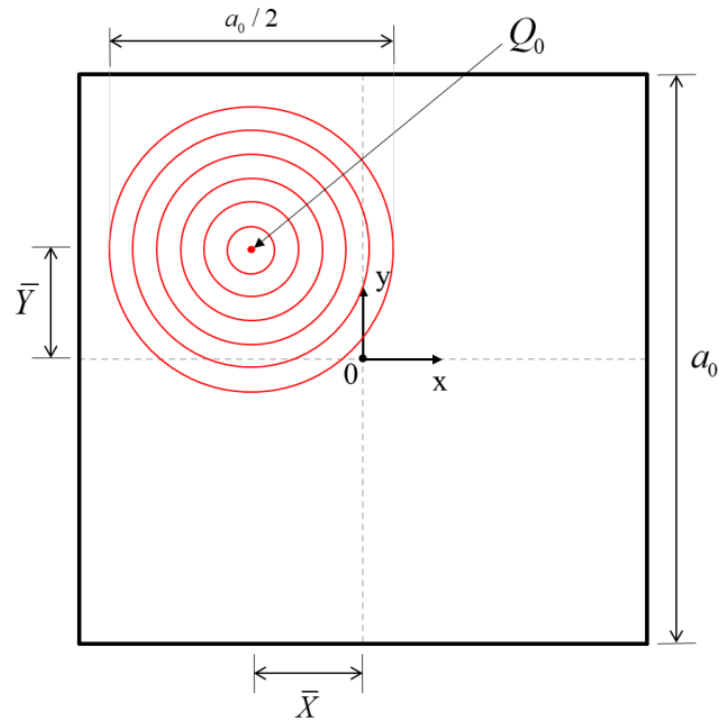
Figure 3.2: Top view of the plate with a two-dimensional representation of an instance of the load on it.
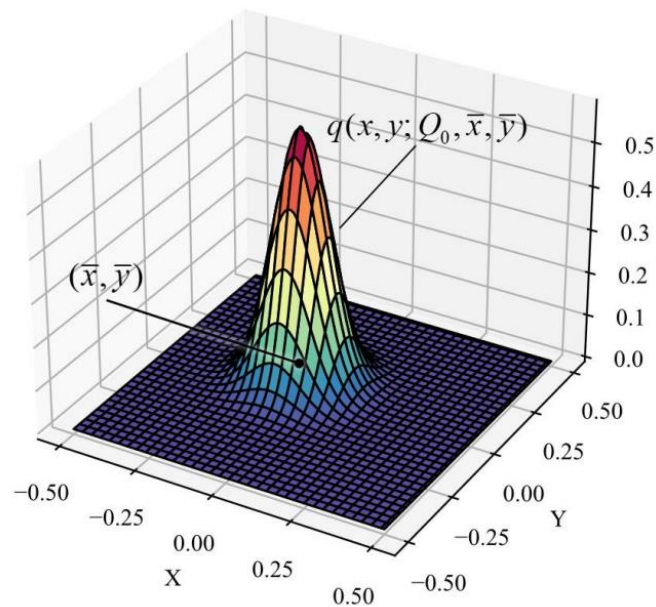
Figure 3.3: 3D representation of an indicative realization of the load profile.

The aforementioned properties are visually summarized in Figure 3.4. The blue crosses correspond to a few thousand instances of sampled load locations. By design, 99.46 % of the load location samples should be corresponding to a point on the plate within the

bounding box. As long as the load's center is sampled within the bounding area, the entirety of the significant part of the load fits on the structural domain.
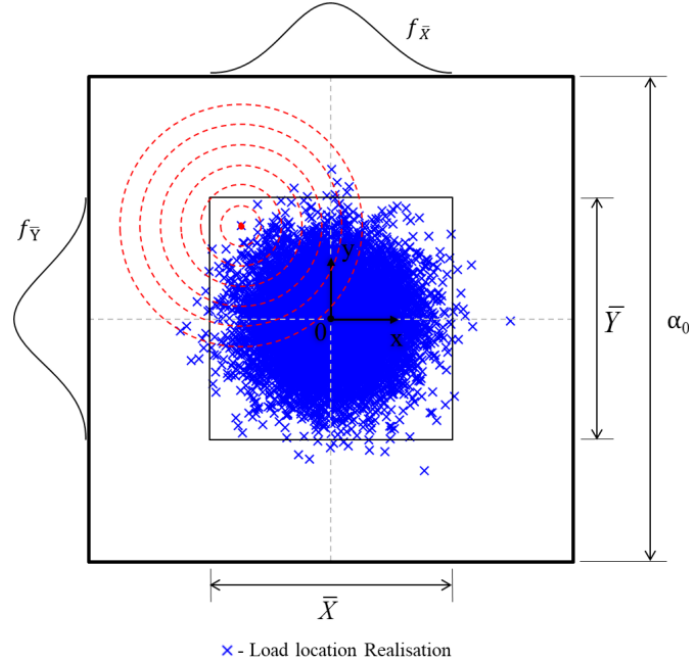
Figure 3.4: Visual representation of realizations of the load location.

The second operational condition that was considered, employed the same pressure profile given by Eq. 3.1, however the parameters $Q_0, \bar{X}, \bar{Y}$ are now considered to be known deterministic constants. In that way, the potential information gain when the loading conditions are not described by stochasticity, is studied.

3.3 Damage Introduction, Sensor Topology and Boundary Conditions

As already presented in the introduction chapter of this thesis, this work revolves around the design of an SHM system that will estimate the corrosion induced thickness loss and associated variability using data collected from strain sensors. Damage is introduced to the problem as global uniform corrosion affecting the entire plate domain and thus it is quite obvious that it can be modeled by reducing uniformly the thickness of the plate. Damage in the present study does not exceed 20% of the nominal thickness of the plate. Considering that the nominal thickness of the plate is 10 mm, the thickness of the corroded plate is examined in an interval [8, 10] mm. More specifically the damage scenario that will be applied is that the plate has lost 15.3% of its nominal thickness. Thus, the thickness value that needs to be inferred is 8.47 mm.

In this work, strain measurements constitute the collected observation data of the inverse problem. Hence, sensor topology is an important aspect of the present analysis. At first a rectangular array of nine equally-spaced strain sensors was considered, i.e., a 3×3 −size sensor grid that is illustrated in Figure 3.5. Every sensor is represented by a gray square mark, while sensors were considered to measure both longitudinal strain components along x and y axis ($\varepsilon_x, \varepsilon_y$), as well as the in-plane shear strain (ε_{xy}) on the plate at a specific location. An observation for the problem would consist of 9 different strain measurements for each component. The initial aim was also to assess the effect

of different grid sizes $(4 \times 4, 5 \times 5, 6 \times 6)$ for each of the components on the information gain about the QoI. Nevertheless, dealing with full grid sensor arrangements posed a tremendous computational cost in order to proceed to Bayesian solutions, making this concept not viable. Thus, it was considered crucial to proceed to dimensionality reduction. Taking as well into account that the plate domain is subjected only to uniform corrosion it was considered possible to find a specific strain sensor location and corresponding component that would account for the solution of the problem (optimal sensor). This specific sensor was selected from the $3 \times 3 -$size sensor grid and how it was selected, would be a subject in the following chapter of the thesis.
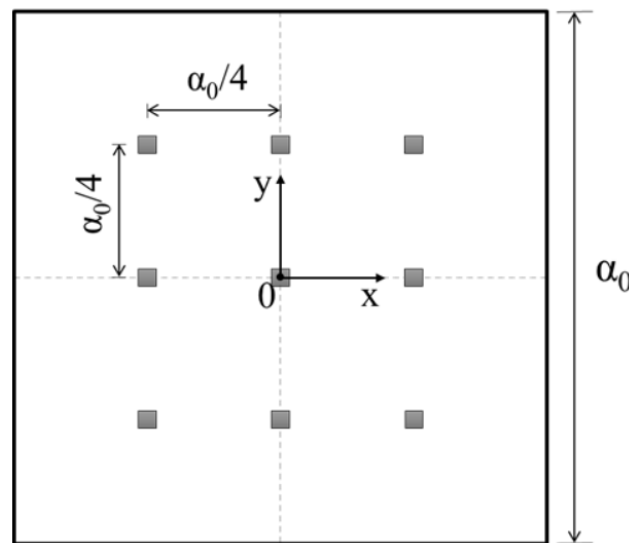
Figure 3.5: 3×3 sensor grid. Each sensor measures longitudinal strain components along x and y axis as well as the in-plane shear strain on the plate.

Finally, regarding the boundary conditions of the plate, it was decided that these will be unsymmetric. Namely, two adjacent sides of the plate were considered as clamped (top and right side) and the other two adjacent sides were considered as simply supported (bottom and left side).

3.4 Finite Element Modeling

A FE model of the plate geometry was generated. The FE model was ultimately intended to serve as a synthetic data generator whereby a computationally cheap surrogate model can be further trained to alleviate its burdensome computational demands. For this purpose, the ANSYS Mechanical commercial software by means of its integrated scripting language (APDL) has been employed. This allowed the model to be parameterized in terms of the input source variability parameters to enable an MCS-based iterative solution scheme. The problem has been cast in a linear static setting with the material being regarded as linear elastic and isotropic, as it was expected that the applied loads would not result in plastic deformation. In this context, a Young's modulus of 207 GPa and a Poisson's ratio of 0.3 were used as representative values of shipbuilding steels.

On the basis that the thickness of the plate was considerably smaller than its other dimensions, it was modeled using four-node rectangular shell elements with six degrees of freedom at each node; three translations along an orthogonal axis system and the respective rotations about these axes. Also 4-node rectangular shell elements (SHELL181) were employed.

Element size was determined by comparing relative solution accuracy between alternative reasonably sized mesh options in three indicative load cases [17]. Based on this comparison an element width of 0.02 m was selected for the FE model provided that it offered accuracy and at the same time would save in required simulation time. As a result, a 50×50-element structured mesh was developed to simulate the rectangular plate. The meshed plate is presented in Figure 3.6.
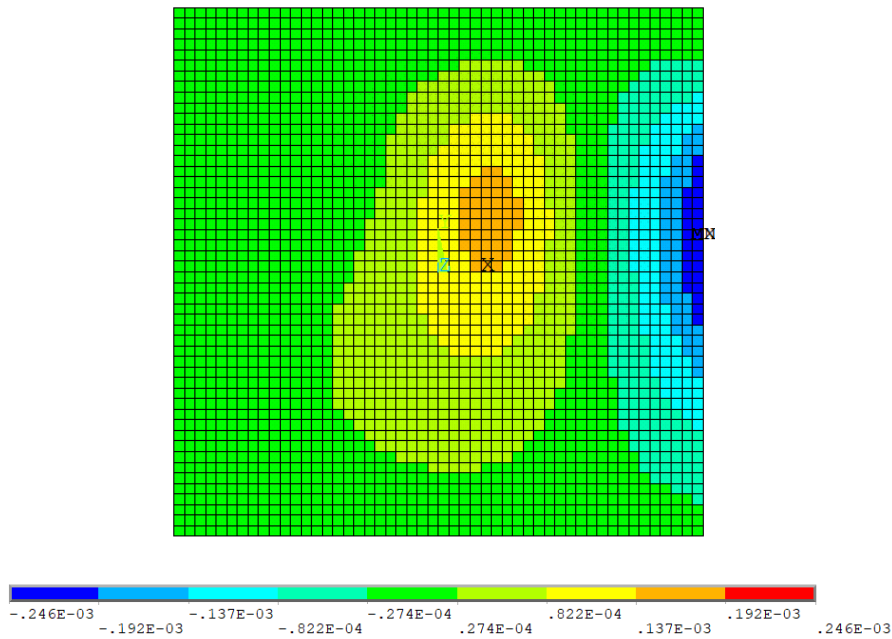
Figure 3.6: Meshed plate and contour plot of the longitudinal (ε_x) strain component on the face of the plate for an indicative pressure load realization.

Concerning the boundary conditions, all degrees of freedom of the nodes along the top and right edge of the plate were restricted to simulate clamped support conditions, whereas translation along the x, y and z axis and rotation about the z axis were restricted for the nodes of bottom and left side to simulate simply supported conditions. The distributed load was applied by discretizing the continuous function that controls its profile. For each load case, the corresponding values of the load magnitude were acquired at the locations of the nodes. More specifically, for a given thickness value denoted by t, the corresponding value of the load (q) at a specific node with coordinates (x_n, y_n), under the given loading scenario $\left(q_0^{(r)}, \bar{x}^{(r)}, \bar{y}^{(r)}\right)$ is calculated as $\left(x_n, y_n, q_0^{(r)}, \bar{x}^{(r)}, \bar{y}^{(r)}\right)$ in accordance with Eq. 3.1.

The FE model was used in order to extract strain measurements in the corroded state and also to generate data for surrogate modeling training using MC sampling.

4 Feature Selection

As already mentioned in the previous section, one needs to proceed to dimensionality reduction by selecting a specific sensor location and strain component from the 3×3 grid, to avoid inefficiency due to high computational cost. In this section the analysis used to select the most insightful sensor for the estimation process is described.

Identifying damage-sensitive features from the collected system response data is generally crucial for the design of a reliable SHM architecture. As it will be discussed in the sections to come, during the process of parameter estimation, strain measurements generated by the high-fidelity FE model are subjected to multiple types of uncertainty, including inherent measurement noise, errors due to load stochasticity as well as prediction errors and surrogate modeling errors. Al these types of errors will be summed and will be considered as a total noise that will describe the uncertainty among the strain data observations. Towards this direction it was considered reasonable to assume that sensor location and strain component that presents the higher strain response as a numerical value and thus is affected less by the total noise, will be the most appropriate feature to proceed with. However, for the sake of completeness and to reassure that sensors with low strain response are not acceptable, the problem will be solved for a sensor that is susceptible to measurement noise as well.

4.1 Stochastic Operational Conditions

In the case of stochastic operational conditions, no specific strain response is available, since the parameters of the pressure profile are treated as random variables. Consequently, the exploration of the optimal feature will be conducted based on the statistical response of the plate domain after repeatedly solving the FE model a great amount of load realizations and thicknesses. The random parameters that define the pressure profile were sampled using MCS from their known distributions given in Section 3.2 while the random thickness' values t were sampled using MCS from a uniform distribution in the interval [8,10]mm. The number of MCS samples was decided to be 10^4 random realizations. This process was carried out for all sensor locations and strain components and the optimal sensor was selected after investigating all different results. Figure 4.1 illustrates the statistical response for three indicative sensor locations and corresponding strain components. Finally, it was decided that ε_y strain measurements generated from sensor 5 of the equally-spaced 3×3 grid arrangement were the least susceptible to noise and thus, the corresponding sensor location and strain component was the optimal feature. Sensor 7 and strain component ε_x was also selected, as the sensor prone to measurement noise.
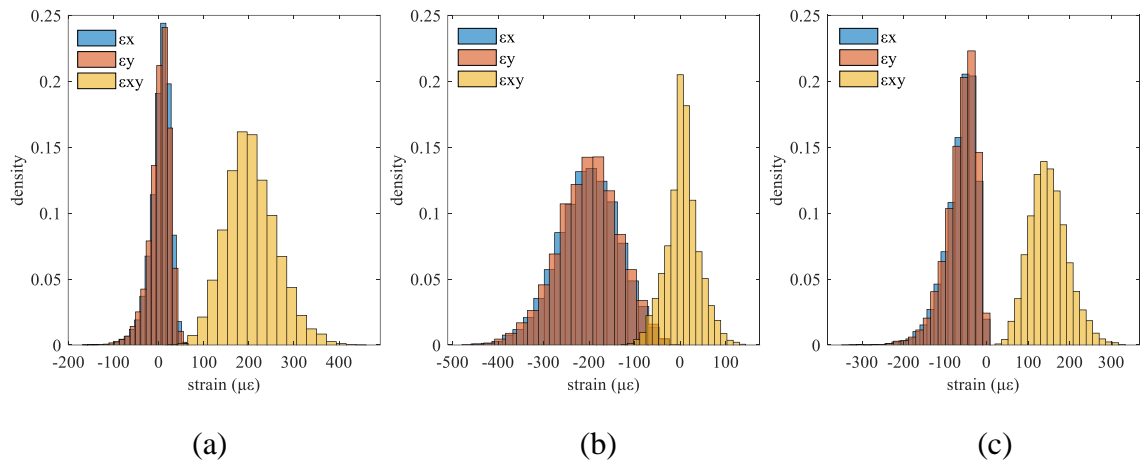
Figure 4.1: Statistical strain response for (a) sensor 3 (b) sensor 5, (c) sensor 7 (3x3 grid).

4.2 Deterministic Operational Conditions

In the case of deterministic operational conditions, the parameters that describe the pressure profile are known constants. Thus, by simulating the FE model in the corroded state the strain response of the plate for this loading condition is given. The strain response is illustrated as a contour plot in Figure 4.2 for all three different strain components. Based on the strain response values, generated from the FE model, on each sensor location and for every strain component, sensor 3 and strain component ε_{xy} describes the optimal feature of the deterministic scenario.
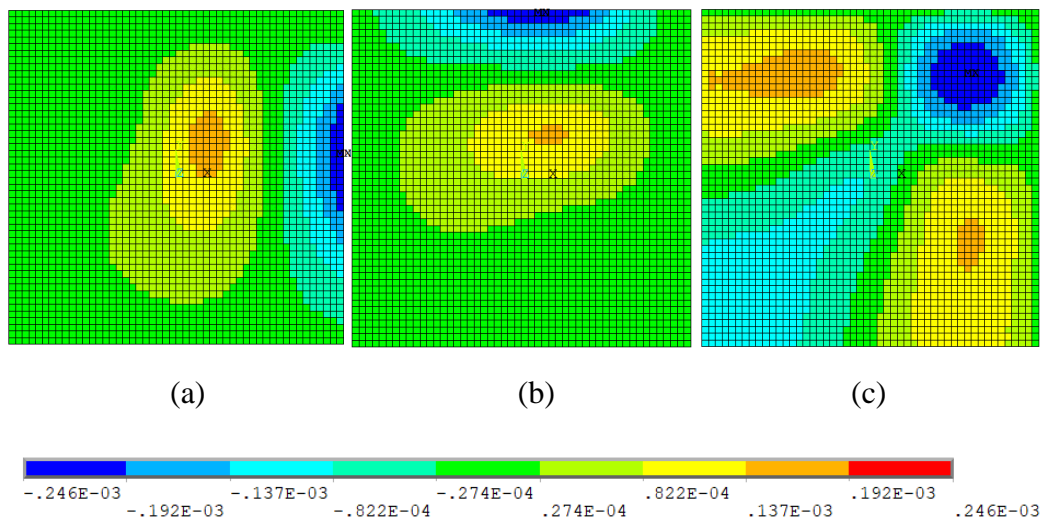
Figure 4.2: Contour plot of strain ε_x (a), ε_y (b) and ε_{xy} (c) for the corroded plate.

5 Bayesian Modeling

In this section uncertainty is introduced to the strain measurements extracted from the high-fidelity FE model. This process set the basis for proceeding to Bayesian inference because one can generate noisy observations for given values of thickness based on a prediction error probability distribution, formulating a probabilistic model in accordance with Section 2.2.2. Furthermore, in this section, the application of surrogate models to the needs of this study, in order to predict strain measurements will be presented before, applying the Bayes theorem to each case.

5.1 Stochastic Operational Conditions

5.1.1 FE-based Engineering Model

The FE model described in the Section 3.4 will represent the engineering model of this problem in accordance with Section 2.1.2. This will be different depending on the operational conditions. Let $\mathcal{M}$ represent the FE model that simulates the behavior of the corroded plate. In the case where load is defined by stochasticity, the model $\mathcal{M}$ is parametrized by $q_0, \bar{x}, \bar{y}, t$. The FE reading ε_{FE} of a strain sensor for a particular strain component when the plate has thickness t can be formulated as follows:

$$\varepsilon_{FE} = \mathcal{M}(q_0, \bar{x}, \bar{y}, t) \qquad \text{Eq. 5.1}$$

Based on Eq. 5.1 it is obvious that this study deals with an inverse UQ problem, where one will be given noisy independent strain measurements and aims to make an inference about the thickness parameter t and its associated uncertainty.

5.1.2 Prediction Error and Surrogate Modeling

Due to load stochasticity, measurement errors, numerical approximations and general inadequacies, strain measurements ε_{FE} from the FE model $\mathcal{M}$ are expected to deviate from real life observations, denoted by ε. Considering the engineering model formulation of the previous section, actual strain measurements can then be interpreted as the following sum:

$$\varepsilon = \varepsilon_{FE} + \eta_p \qquad \text{Eq. 5.2}$$

$$\varepsilon = \mathcal{M}(q_0, \bar{x}, \bar{y}, t) + \eta_p \qquad \text{Eq. 5.3}$$

Where η_p is the prediction error that describes the discrepancy between the model measurements ε_{FE} and the actual experimental data ε. In this work, this error contains the uncertainty not only due to FE modeling errors but also due to inherent randomness of the problem representing both epistemic uncertainty and aleatoric variability of the system.

However, in order to proceed to Bayesian inference by applying the MCMC algorithm, the FE model needs to be called a great number of times independently each time a new candidate of the thickness parameter is sampled from the proposal distribution. Consequently, the algorithm tends to be inefficient. With the intention of overcoming

this obstacle a surrogate model $\widehat{\mathcal{M}}$ is employed to cope with the iterative nature of the MCMC algorithms. Given the input parameters $q_0, \bar{x}, \bar{y}, t$ the surrogate models proceed to make a prediction about the strain measurement ε_{FE}. This prediction strain measurement is denoted by $\hat{\varepsilon}$, and is formulated as follows:

$$\hat{\varepsilon} = \widehat{\mathcal{M}}(q_0, \bar{x}, \bar{y}, t) \qquad \text{Eq. 5.4}$$

For the needs of stochastic operational conditions, the surrogate model needs to be trained taking four parameters $q_0, \bar{x}, \bar{y}, t$ as inputs and one parameter ε_{FE} as output in the training process. The stochastic nature of the load causes simple regression models to be unsuitable as surrogate models for the case. Consequently, Gaussian support vector regression was employed.

In order to create the baseline D^{base} of the synthetic data that would be used for training and testing, the 10^4 realizations and strain results that were used in strain statistical response, were employed. Namely, the base set was formulated as $D^{base} = \{q_{0_m}, \bar{x}_m, \bar{y}_m, t_m; \varepsilon_{FE_m}\}$, where $m = 1, \dots, 10^4$. From the total number of points in D^{base}, 80% were assigned for training and 20% for testing purposes. The training D^{train} and testing D^{test} datasets were ensured to be mutually exclusive to avoid compromising the measure of generalization of the surrogate.

During the process of estimating the SV regression hyperparameters, a k-fold cross validation process of 5 folds was conducted. To achieve that, the entire available data set was split into 5 sets and the model was trained using the data from all except one (i.e., 4 out of the 5 sets), while the remaining one was used for validation. This was repeated for all 5 possible validation sets and the final validation score was obtained as the average of their respective scores. Furthermore, in order to assess the performance of the surrogate model the metric coefficient of determination, known as R^2, was employed. In general, the larger the R^2 is, the higher the accuracy of the trained model is, and a value larger than 0.8 is believed to represent a high degree of accuracy. The value of R^2 between surrogate strain predictions and their corresponding targets from the FE model ε_{FE}, is defined as:

$$R^2 = 1 - \frac{\sum_{m=1}^{M}\left(\widehat{\varepsilon_m} - \varepsilon_{FE_m}\right)^2}{\sum_{m=1}^{M}\left(\bar{\varepsilon} - \varepsilon_{FE_m}\right)^2} \qquad \text{Eq. 5.5}$$

Where M is the size of D^{test}, ε_{FE_m} is the mth strain observation from the FE model and $\widehat{\varepsilon_m}$ is the corresponding predicted output from the surrogate model. As an indicative case, the score for the optimal sensor is presented in Figure 5.1. From the performance of the R^2, it can be observed that the model has been trained effectively and that a sufficiently high performance has been achieved for the surrogate model ($R^2 = 0.998$).
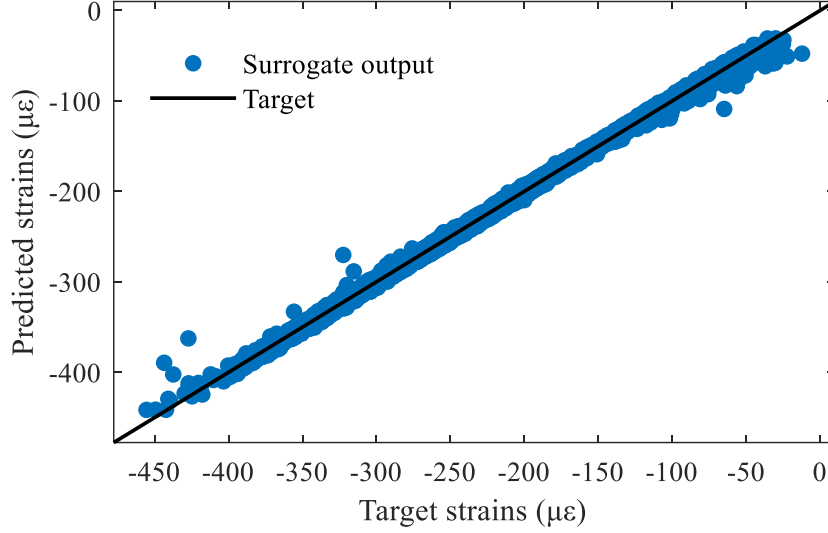
Figure 5.1: Indicative regression fit representing the R^2 score of the surrogate model.

Nevertheless, no matter how good R^2 score does the surrogate model have, there always an error in the predictions. The surrogate model error is formulated as follows:

$$\eta_s = \varepsilon_{FE} - \hat{\varepsilon} \qquad \text{Eq. 5.6}$$

Combining Eq. 5.2 with Eq. 5.6, one can proceed to the formulation of the model that relates the real strain observations ε with the ones generates from the surrogate model $\hat{\varepsilon}$ as shown in Eq. 5.8 . This model will be used in the Bayesian framework.

$$\varepsilon = \hat{\varepsilon} + \eta_p + \eta_s \qquad \text{Eq. 5.7}$$

$$\varepsilon = \widehat{\mathcal{M}}(q_0, \bar{x}, \bar{y}, t) + \eta \qquad \text{Eq. 5.8}$$

Where the term $\eta = \eta_p + \eta_s$ accounts for all types of modeling errors and measurements uncertainties and is considered to be random variable. This residual term is treated as a Gaussian zero-mean random variable with a user-specified variance; namely $H \sim p_H(\eta; \sigma)$, with $p_H(\eta; \sigma) = \mathcal{N}(0, \sigma)$. It should be noted that the residual parameter σ is considered to be unknown and is included in the parameters to be inferred with Bayesian modeling. As it will be clear in Section 5.1.3 the residual term constitutes the probabilistic model in accordance with Section 2.2.2, that one can use in order to explain the randomness of the data for given parameter values and it will be used to formulate the likelihood function of the problem.

5.1.3 Bayesian Formulation

In this section the process followed to apply the Bayes theorem will be described.

Prior Model and Input Uncertainty

In Bayesian fashion the unknown QoI are treated as random variables. Namely for the present problem, a prior distribution $\pi(t)$ is assigned to the thickness parameter t as follows:

$$T \sim \pi(t) \qquad \text{Eq. 5.9}$$

The Bayesian prior distribution quantifies a subjective degree of plausibility or belief about the true parameter values t. For this work, two different prior distributions for the thickness parameter were examined. The first will be an uninformative uniform prior distribution, whereas the second will be a more biased prior that will be selected based on statistical data from existing corrosion situations on the bottom of ships. The biased prior will be treated as a normal prior distribution.

It should be noted that according to the previous section, the residual parameter σ is also included in the parameters to be inferred. Thus, another uninformative uniform prior distribution is assigned to this parameter:

$$\Sigma \sim \pi(\sigma) \qquad\qquad \text{Eq. 5.10}$$

A vector θ is then considered, that contains all the parameters that need to be inferred. Thus, θ is a two-dimensional vector, containing both plate thickness t and the standard deviation of the residual model σ, i.e., $\theta = \{t, \sigma\}^T$. These parameters are considered to be independent. Consequently, the joint prior distribution $\pi(\theta)$ can be written as the product of the two independent prior distributions:

$$\pi(\theta) = \pi(t, \sigma) = \pi(t)\pi(\sigma) \qquad\qquad \text{Eq. 5.11}$$

Probabilistic Model and Likelihood Function

Based on the residual term formulation in Eq. 5.8, actual strain observations viewed as outcomes ε_i of random variable:

$$(E_i | Q_0 = q_0, \bar{X} = \bar{x}, \bar{Y} = \bar{y}, T = t) \sim p_H(\varepsilon_i - \widehat{\mathcal{M}}(q_0, \bar{x}, \bar{y}, t); \sigma) \qquad \text{Eq. 5.12}$$

Thus, the observation data set of the problem is generated by independently sampling from the distribution of Eq. 5.12. The total number of observations was considered to be $n = 100$ strain measurements. The measurements were generated initially, using a standard deviation level of $5\mu\varepsilon$, however different measurement noise levels will be also examined.

Namely, for given values of the direct forward model input $q_0, \bar{x}, \bar{y}, t$, data are viewed as random variables $(E_i | q_0, \bar{x}, \bar{y}, t)$ with conditional distribution:

$$p(\varepsilon_i | q_0, \bar{x}, \bar{y}, t ; \sigma) = p_H(\varepsilon_i - \widehat{\mathcal{M}}(q_0, \bar{x}, \bar{y}, t); \sigma) \qquad\qquad \text{Eq. 5.13}$$

The model of Eq. 5.13 refers to a single observation. In order to formulate a conditional distribution for the total n generated independent data $\langle \varepsilon_i \rangle$ for given values of the unknown parameters $q_0, \bar{x}, \bar{y}, t$, the following product is taken:

$$p(\langle \varepsilon_i \rangle | q_0, \bar{x}, \bar{y}, t ; \sigma) = \prod_{i=1}^{n} p(\varepsilon_i | q_0, \bar{x}, \bar{y}, t; \sigma) \qquad\qquad \text{Eq. 5.14}$$

Bayesian Modeling

$$\Rightarrow p(\langle \varepsilon_i \rangle \,|q_0, \bar{x}, \bar{y}, t\,; \sigma) = \prod_{i=1}^{n} p_H(\varepsilon_i - \widehat{\mathcal{M}}(q_0, \bar{x}, \bar{y}, t); \sigma) \qquad \text{Eq. 5.15}$$

Thus, the connection between the observation data $\langle \varepsilon_i \rangle$ and the unknown input QoI that are contained in the parameter vector θ is established, and the probabilistic model is constructed in accordance with Section 2.2.2. Based on the aforementioned, one can then formulate the likelihood function of the vector parameter θ, for a single observation (Eq. 5.16) and for the total observation data (Eq. 5.17).

$$\mathcal{L}(\theta|\varepsilon_i) = p(\varepsilon_i|\theta) \qquad \text{Eq. 5.16}$$

$$\mathcal{L}(\theta|\langle \varepsilon_i \rangle) = \prod_{i=1}^{n} p(\varepsilon_i|\theta) \qquad \text{Eq. 5.17}$$

In Bayesian problems and MCMC algorithms, the log-likelihood function is commonly employed for practical issues, such as treating the product for the total observations data as a sum. Hence, the log-likelihood is formulated above, and Eq. 5.16 and Eq. 5.17 are developed to Eq. 5.18 and Eq. 5.19 accordingly.

$$log\, \mathcal{L}(\theta|\varepsilon_i) = log\, p(\varepsilon_i|\theta) \qquad \text{Eq. 5.18}$$

$$log\, \mathcal{L}(\theta|\langle \varepsilon_i \rangle) = \sum_{i=1}^{n} log\, p(\varepsilon_i|\theta) \qquad \text{Eq. 5.19}$$

It is obvious that the likelihood function of the problem refers only to the parameter vector θ, which contains the QoI, and therefore in order to use the constructed probabilistic model of Eq. 5.13, the influence of the load related parameters $q_0, \bar{x}, \bar{y}$ on the output of the surrogate model $\widehat{\mathcal{M}}$ has to be accounted for, by marginalizing the likelihood over their corresponding domains $D_{q_0}, D_{\bar{x}}, D_{\bar{y}}$. Consequently, the quantity $p(\varepsilon_i|\theta)$ is formulated by marginalization as follows:

$$p(\varepsilon_i|\theta) = \int_{D_{q_0}} \int_{D_{\bar{x}}} \int_{D_{\bar{y}}} p_H(\varepsilon_i - \widehat{\mathcal{M}}(q_0, \bar{x}, \bar{y}, t); \sigma)\, dq_0\, d\bar{x}\, d\bar{y} \qquad \text{Eq. 5.20}$$

The process of calculating the multidimensional integral in Eq. 5.20 is difficult to be performed analytically. This leads to the approximation of the integral and the likelihood function as a whole, through Monte Carlo integration. According to Monte Carlo integration, an approximation $\hat{p}(\varepsilon_i|\theta)$ of the multidimensional integral of Eq. 5.20 is given by Eq. 5.21:

$$\hat{p}(\varepsilon_i|\theta) = \frac{1}{K} \sum_{k=1}^{K} p_H(\varepsilon_i - \widehat{\mathcal{M}}(q_0, \bar{x}, \bar{y}, t); \sigma) \qquad \text{Eq. 5.21}$$

Where K is the number of independently sampled forward model inputs $q_0, \bar{x}, \bar{y}$. The samples are generated from their probability distributions as presented in Section 3.2. Consequently, the following approximation of the marginalized likelihood over all observation data is formulated and will be used in the Bayesian problem:

$$log\ \hat{\mathcal{L}}(\theta|\langle\varepsilon_i\rangle) = \sum_{i=1}^{n} log\ \hat{p}(\varepsilon_i|\theta) \qquad \text{Eq. 5.22}$$

In order to select the appropriate number of samples K for the integral approximation in Eq. *2.21*, a convergence study was conducted, and the results are presented in Figure 5.2, for an indicative θ. Based on Figure 5.2 and considering that the marginalization process develops an additional computational cost to the Bayesian estimation problem, a number of 1500 samples was considered adequate to achieve convergence.
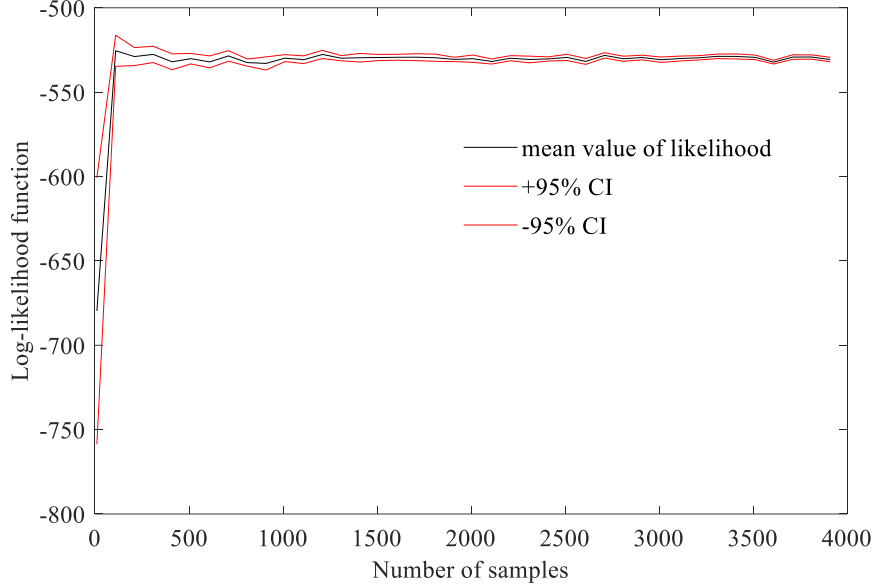
Figure 5.2: Convergence diagram for the Monte Carlo integration. The red lines represent the 95% confidence intervals.

Bayes Theorem

Having set the prior model and constructed the likelihood function, one can proceed to the joint posterior probability function of the unknown parameters $\theta = \{t, \sigma\}^T$ by conditioning on the observations data $\langle\varepsilon_i\rangle$ according to the Bayes theorem (see Eq. 5.23). For the sake of simplicity, the Bayes theorem is presented using the likelihood function and not the log-likelihood function.

$$p(\theta|\langle\varepsilon_i\rangle) = \frac{1}{C}\pi(\theta)\hat{\mathcal{L}}(\theta|\langle\varepsilon_i\rangle) \qquad \text{Eq. 5.23}$$

The term C is the model evidence, given by Eq. 5.24, where D_t, D_σ are the corresponding domains of thickness and standard deviation accordingly.

$$C = \int_{D_t}\int_{D_\sigma}\pi(\theta)\hat{\mathcal{L}}(\theta|\langle\varepsilon_i\rangle)\ dt\ d\sigma \qquad \text{Eq. 5.24}$$

In order to proceed to parameter estimation and uncertainty quantification using Eq. 5.25 the term C needs to be omitted as discussed in Section 2.3.1. This will be achieved by applying the MH algorithm, in order to sample from the joint posterior distribution.

5.2 Deterministic Operational Conditions

5.2.1 FE Based Engineering Model

Similar to stochastic loading, in the deterministic load scenario the FE model will represent the engineering model of this problem. However, this time the quantities $q_0, \bar{x}, \bar{y}$ are considered known constants, and thus the model $\mathcal{M}$ is only parametrized by the thickness of the plate t. The FE reading ε_{FE} of a strain sensor for a particular strain component is given by Eq. 5.25

$$\varepsilon_{FE} = \mathcal{M}(t) \qquad \text{Eq. 5.25}$$

5.2.2 Prediction Error and Surrogate Modeling

Real strain measurements ε are expected to deviate from the measurements generated from the FE model, just like in stochastic operational conditions. As such actual strain measurements can then be interpreted as the following sum:

$$\varepsilon = \mathcal{M}(t) + \eta_p \qquad \text{Eq. 5.26}$$

Where η_p is again the prediction error that describes the discrepancy between the model measurements ε_{FE} and the actual experimental data ε representing epistemic uncertainty and aleatoric variability.

A surrogate model $\widehat{\mathcal{M}}$ will again be trained next in order to cope with the iteration nature of MCMC algorithm. However, while the output of the model remains the strain measurement ε_{FE}, the input parameter in this case is just plate thickness t, namely the model is much simpler than the previous case. This fact allows simpler regression models to be suitable for the deterministic loading case. Specifically, a second-degree polynomial is employed and only eight training points $\{t, \varepsilon_{FE}\}$ were considered adequate to achieve regression with high efficiency. Figure 5.3 illustrates the training data points and the corresponding regression second degree polynomial curve for the optimal sensor feature of this case. Predictions $\hat{\varepsilon}$ are estimated in accordance with Eq. 5.27. The metric coefficient R^2 was also employed in this case, and the score resulted in an $R^2 = 0.999$, achieving efficiency of the surrogate.

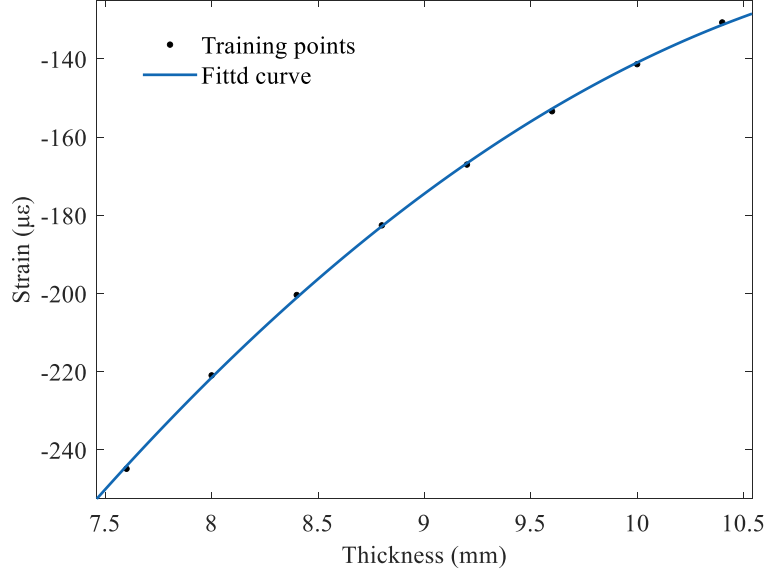$$\hat{\varepsilon} = \widehat{\mathcal{M}}(t) \qquad \text{Eq. 5.27}$$

Figure 5.3: Training data points and corresponding regression curve for the optimal sensor of the deterministic load scenario.

Similar to the stochastic loading scenario, the surrogate modeling error is formulated next, i.e., $\eta_s = \varepsilon_{FE} - \hat{\varepsilon}$, and combining it with Eq. 5.26 one can proceed to the formulation of the model that relates the real strain observations ε with the ones generates from the surrogate model $\hat{\varepsilon}$, as shown in Eq. 5.28. This model will be used in the Bayesian framework.

$$\varepsilon = \widehat{\mathcal{M}}(t) + \eta \qquad \text{Eq. 5.28}$$

Where the term $\eta = \eta_p + \eta_s$ accounts for all types of modeling errors and measurements uncertainties and is considered to be random variable. This residual term is treated again as a Gaussian zero-mean random variable with a user-specified variance; namely $H \sim p_H(\eta; \sigma)$, with $p_H(\eta; \sigma) = \mathcal{N}(0, \sigma)$. The residual parameter σ is considered to be unknown and is included in the parameters to be inferred with Bayesian modeling.

5.2.3 Bayesian Formulation

Prior Model and Input Uncertainty

The prior models in the case of the deterministic operational conditions appear to have no difference compared to the ones in the stochastic operational conditions. Thus, no further analysis is presented regarding prior models and the reader is referred to the corresponding Section 5.1.3.

Probabilistic Model and Likelihood Function

Based on the residual term formulation in Eq. 5.28, actual strain observations viewed as outcomes ε_i of random variable:

$$(E_i|T = t) \sim p_H(\varepsilon_i - \widehat{\mathcal{M}}(t); \sigma) \qquad \text{Eq. 5.29}$$

Thus, the observation data of the problem are generated by independently sampling from the distribution of Eq. 5.29, and the number of these data was considered to be again $n = 100$ strain measurements. The measurements were generated, using a standard deviation level of $5\mu\varepsilon$.

Namely, for given values of the direct forward model input t, data are viewed as random variables $(E_i|\ t)$ with conditional distribution:

$$p(\varepsilon_i|t\ ;\sigma) = p_H(\varepsilon_i - \widehat{\mathcal{M}}(t);\sigma) \qquad \text{Eq. 5.30}$$

The model of Eq. 5.30 refers to a single observation. In order to formulate a conditional distribution for the total n generated independent data $\langle\varepsilon_i\rangle$ for given values of the unknown parameter t ,the following product is taken:

$$p(\langle\varepsilon_i\rangle\ |t\ ;\sigma) = \prod_{i=1}^{n} p(\varepsilon_i|t;\sigma) \qquad \text{Eq. 5.31}$$

$$\Rightarrow p(\langle\varepsilon_i\rangle\ |t\ ;\sigma) = \prod_{i=1}^{n} p_H(\varepsilon_i - \widehat{\mathcal{M}}(t);\sigma) \qquad \text{Eq. 5.32}$$

Thus, the connection between the observation data $\langle\varepsilon_i\rangle$ and the unknown input QoI that are contained in the parameter vector θ is once again established, and the probabilistic model is constructed in accordance with Section 2.2.2. Based on the aforementioned, one can then formulate the likelihood function of the vector parameter θ, for a single observation (Eq. 5.33) and for the total observation data (Eq. 5.34)

$$\mathcal{L}(\theta|\varepsilon_i) = p(\varepsilon_i|\theta) \qquad \text{Eq. 5.33}$$

$$\mathcal{L}(\theta|\langle\varepsilon_i\rangle) = \prod_{i=1}^{n} p(\varepsilon_i|\theta) \qquad \text{Eq. 5.34}$$

Similar to the stochastic case, the log-likelihood function is then employed for practical issues. Hence, the log-likelihood is formulated above, and Eq. 5.33 and Eq. 5.34 are developed to Eq. 5.35 and Eq. 5.36 accordingly.

$$log\ \mathcal{L}(\theta|\varepsilon_i) = log\ p(\varepsilon_i|\theta) \qquad \text{Eq. 5.35}$$

$$log\ \mathcal{L}(\theta|\langle\varepsilon_i\rangle) = \sum_{i=1}^{n} log\ p(\varepsilon_i|\theta) \qquad \text{Eq. 5.36}$$

In the deterministic case, the constructed probabilistic model of strain observations, only refers to the parameter vector θ which contains the parameters of interest. Therefore, in this case no further marginalization of the likelihood function is necessary and one can proceed to the application of the Baye's theorem directly.

Bayes Theorem

Having set the prior model and constructed the likelihood function, one can proceed to the joint posterior probability function of the unknown parameters $\theta = \{t, \sigma\}^T$ by conditioning on the observations data $\langle \varepsilon_i \rangle$ according to the Bayes theorem (Eq. 5.37). For the sake of simplicity, the Baye's theorem is presented using the likelihood function and not the log-likelihood function.

$$p(\theta|\langle \varepsilon_i \rangle) = \frac{1}{C}\pi(\theta)\mathcal{L}(\theta|\langle \varepsilon_i \rangle)$$

<div align="right">Eq. 5.37</div>

The term C is the model evidence, given by Eq. 5.38, where D_t, D_σ are the corresponding domains of thickness and standard deviation accordingly.

$$C = \int_{D_t} \int_{D_\sigma} \pi(\theta)\mathcal{L}(\theta|\langle \varepsilon_i \rangle)\, dt\, d\sigma$$

<div align="right">Eq. 5.38</div>

Once again, in order to proceed to parameter estimation and uncertainty quantification using Eq. 5.38 the term C needs to be omitted as discussed in Section 2.3.1. This will be achieved by applying the MH algorithm, in order to sample from the joint posterior distribution.

6 Metropolis Algorithm and Results

In the present chapter the MH algorithm is applied to the Bayesian problem of this study in order to extract posterior samples for the QoI. Convergence diagnostics are examined, and parameter estimation is performed by calculating the mode of the posterior distribution as a point estimate, while the associated uncertainty is quantified by taking the 95% credible interval.

6.1 Numerical Prerequisites

Before proceeding to the application of the algorithm, a reminder regarding the numerical data for the specific problem will be presented in this section. The plate of interest is subjected to corrosion under both deterministic and stochastic operational conditions and has lost 15.3% of its nominal thickness. A total number of 100 strain measurements are generated from specific sensor locations and components on the plate in order to make estimation about the thickness of the corroded plate, i.e., $t_{target} = 8.47\ mm$. At the same time the probabilistic model constructed to proceed to Bayesian inference posed another parameter of interest, which is the standard deviation σ of the residual error term η. The target value of the parameter of standard deviation is set to $\sigma_{target} = 5\ \mu\varepsilon$. Consequently, the target parameter vector is considered as follows:

$$\theta_{target} = \{8.47, 5\}^T \qquad \text{Eq. 6.1}$$

Furthermore, prior distribution needs to be selected for the parameter vector θ. With respect to the thickness parameter, a uniform distribution in the interval [8, 10] mm will represent the uninformative prior, i.e., $\pi(t) = U(8,10)$, while a normal distribution will represent the more biased prior, i.e., $\pi(t) = \mathcal{N}(8.6,0.1)$. The parameters of the biased prior have occurred based on statistical data from existing corrosion measurements on the bottom of bulk carriers [65]. As regards the standard deviation σ, uninformative prior in an interval [1,30] με is selected, i.e., $\pi(\sigma) = U(1,30)$. Considering that the two parameters are independent, the total prior of the problem is formulated as discussed in Section 5.1.3:

$$\pi(\theta) = \pi(t, \sigma) = \pi(t)\pi(\sigma) \qquad \text{Eq. 6.2}$$

In the Metropolis algorithm a proposal distribution needs to be considered, that will suggest a candidate as a next sample in order to be accepted or rejected according to the Metropolis correction step, as discussed in Section 2.3.4. In Random Walk Metropolis sampling, that is applied in the present study a symmetrical multivariate normal distribution is selected, i.e., $q(\theta^{(*)}|\theta^j) = \mathcal{N}(\theta^{(*)}; \theta^j, \Sigma_p)$, where, by $\theta^{(*)}$ is denoted the suggested from the proposal candidate, θ^j the current chain state at iteration j and Σ_p the covariance matrix of the proposal distribution. The covariance matrix of the proposal distribution will be considered after investigating the MCMC trace plots and the corresponding acceptance rates for different values of the matrix. After this process the following covariance matrix was considered acceptable:

$$\Sigma_p = \begin{bmatrix} 0.04 & 0 \\ 0 & 0.5 \end{bmatrix} \qquad \text{Eq. 6.3}$$

Finally, it should be noted that the Metropolis algorithm was applied in order to generate a total number of 11000 samples, from which the first 1000 were discarded as the Burn-In period. Consequently, a total number of 10000 samples from the posterior distributions were generated for each targeted parameter.

6.2 Stochastic Operational Conditions

Results with respect to stochastic operational conditions are presented in this section.

6.2.1 Convergence Diagnostics and Autocorrelation

According to the theory discussed in sections 2.3.6 and 2.3.5 respectively, convergence of the chain created by the Metropolis algorithms, as well as autocorrelation need to be investigated. Convergence will be verified by evaluating the mixing and stationarity in trace plots, while autocorrelation will be illustrated in ACF graphs. For the convergence assessment three chains, each with a different initial point, were created.

<u>Optimal Sensor</u>

Figure 6.1 illustrates the trace plots for both parameters of thickness and standard deviation for the optimal sensor feature. With regard to the thickness parameter, it can be observed that all the chains have mixed adequately and reached stationarity. The chains are moving fast, and they are exploring the entire sample space around the true value of the parameter. On the other hand, regarding the parameter of standard deviation of the residual model, it is obvious, that despite the fact that all the three chains have adequately converged to a stationary distribution, this distribution is different depending on the initial point and none of these distributions seems to contain the true value of the parameter. The chains have not mixed, and general convergence is not achieved. Hence, no valid inference can be conducted with respect to the standard deviation of the error model. This is not something unexpected, due to the marginalization process that is applied in this case. The marginalization process is performed over the loading parameters $q_0, \bar{x}, \bar{y}$, which along with the parameter of thickness t determine the mean value of the constructed probabilistic model. Thus, by applying the process, the behavior of the mean is dominant, while the information regarding the spread of distribution, i.e., the standard deviation σ is fading. Therefore, the likelihood function appears to be flat, with respect to the standard deviation parameter which leads to the parameter not being easily identifiable.

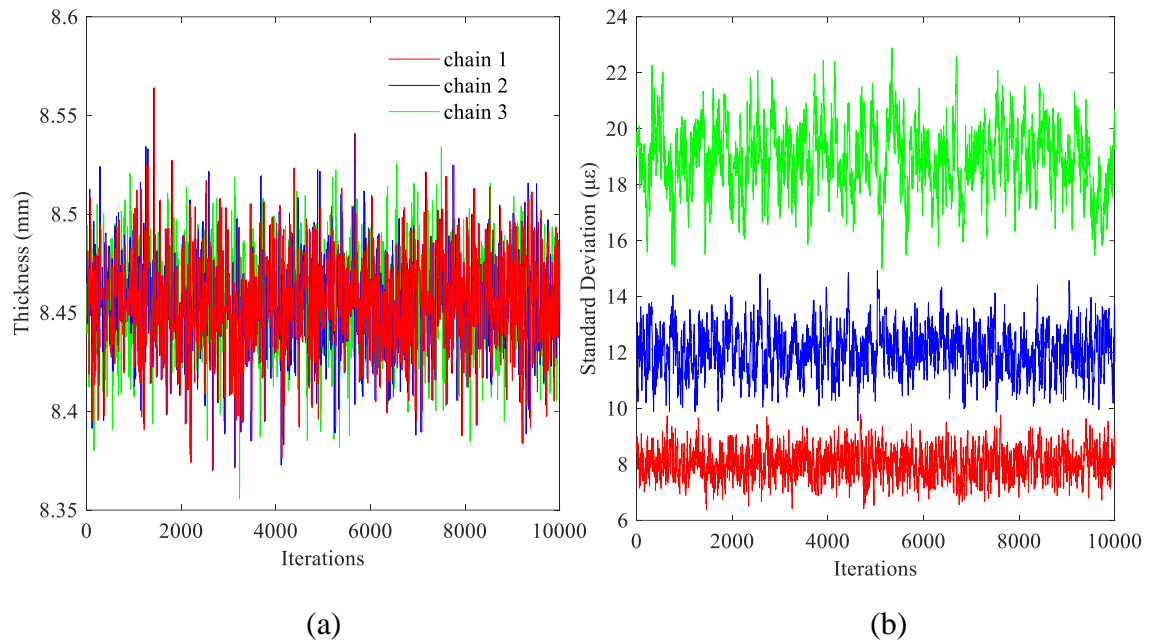(a)   (b)

Figure 6.1: Trace plots showing the trajectory of the chains for the optimal sensor under stochastic operational conditions, for the parameter of (a) thickness and (b) standard deviation.

Figure 6.2 contains the ACF graph illustrating the samples autocorrelation behavior over different lag values for the thickness of the plate. It should be noted that since the chains of standard deviation parameter have not converged to a stationary distribution, there is no point in plotting the corresponding ACF graph for this parameter. Based on Figure 6.2, it is observed that the autocorrelation between samples is large at short lags, but decays quickly to zero as the lag number increases, considering acceptable autocorrelation behavior. It should be also noted that the acceptance rate in this case is approximately 34%.
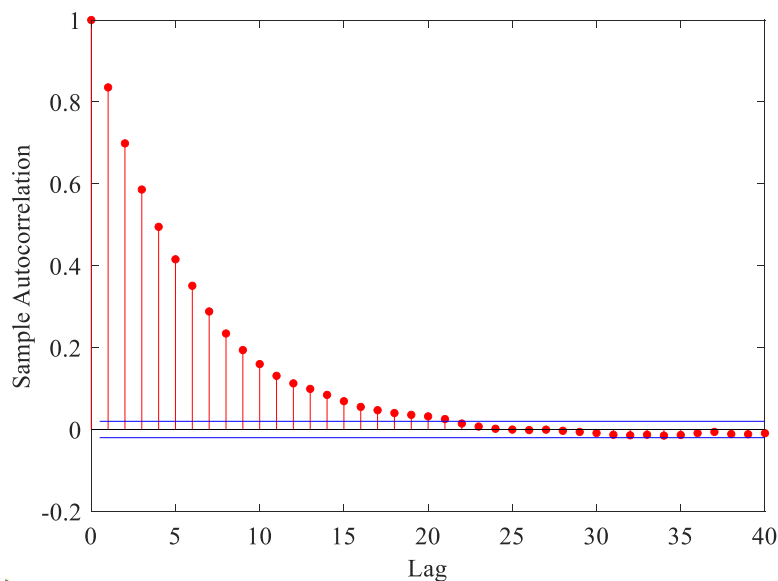

Figure 6.2: Correlogram for the parameter of thickness for the optimal sensor under stochastic operational conditions.

57

Noise-Sensitive Sensor

Figure 6.3 illustrates the trace plots for the parameter of thickness for the sensor that it is prone to measurement errors. Based on this figure, it can be seen that chains are generally exploring the sample space around values that are close to the targeted thickness value and that they are mixed with each other. Nevertheless, each chain appears to get stuck very often for many iterations and does not explore the whole sample space adequately, resulting in high serial correlation between samples. This can be as well verified by the corresponding correlogram illustrated in Figure 6.4. Acceptance rate in this case drops to 6%. The sensor's noise-sensitivity results in an inevitable high correlation, which cannot be accepted in order to make valid estimations about the target parameter.
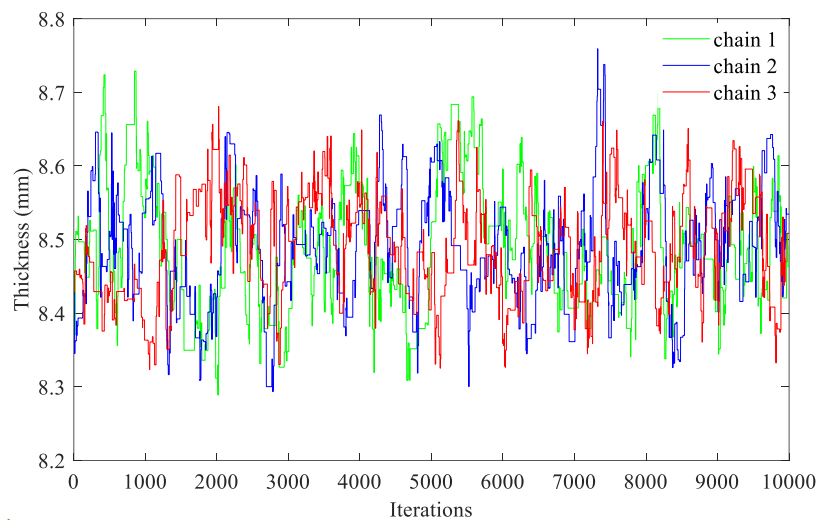
Figure 6.3: Trace plot showing the trajectory of the chains for the noise-sensitive sensor, for the parameter of thickness.
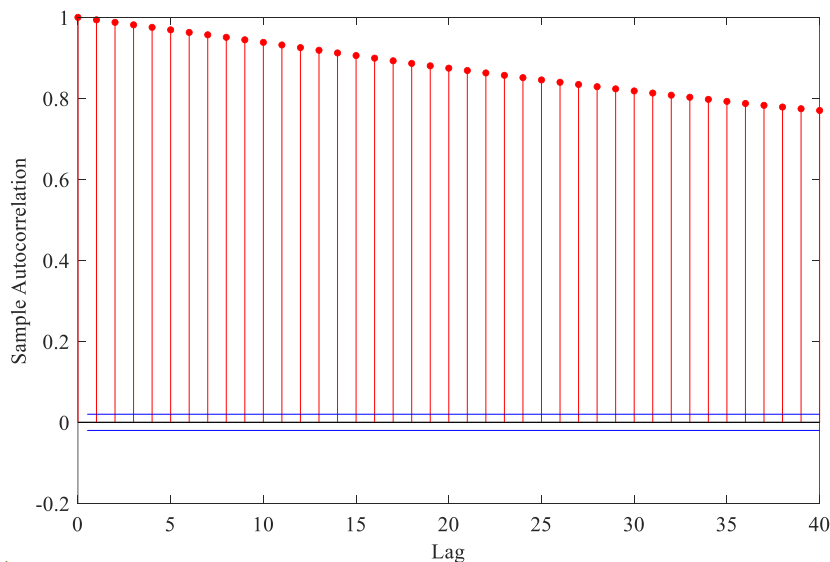
Figure 6.4: Correlogram for the parameter of thickness for the noise-sensitive sensor.

6.2.2 Marginal Posterior Distributions

After evaluating the convergence of the MCMC process, one can proceed to the development of the marginal posterior distributions based on the generated samples and calculate the mode of the distribution, as well as the 95% credible interval, which represent the point estimation of the target parameter and the corresponding uncertainty accordingly. These results are presented for the optimal sensor since, it is the only one that can produce valid inferences and will regard only the parameter of thickness, since chains for the standard deviation have not achieved convergence.

Uninformative Uniform Prior

Figure 6.5 illustrates the marginal posterior distribution for the thickness parameter along with a corresponding Q-Q plot when a uniform prior is applied, where it can be clearly observed that the distribution can be approximately described by a normal distribution. Furthermore, Table 1 contains the value of the point estimated thickness and the corresponding 95% credible interval. It is obvious that the method achieves a very good estimation of the targeted thickness with a relatively small uncertainty regardless of the fact that no prior knowledge is applied.

(a)   (b)

Figure 6.5: (a) Histogram of the posterior distribution of thickness for the optimal sensor under stochastic operational conditions, (b) corresponding Q-Q plot. (Uniform Prior).

Table 6.1: Parameter estimations for the optimal sensor under stochastic operational conditions. (Uniform Prior).

Parameter	Target Value	Point Estimate	% Difference	Credible Interval
t (mm)	8.47	8.46	0.12	[8.42, 8.49]
σ (με)	5	-		-

Informative Normal Prior

Similarly, Figure 6.6 and Table 6.2 sum up the estimation results when the informative normal prior is applied. It appears that the posterior distribution has the exact same behavior and that point estimates do not diverge from the estimates based on the uniform prior, meaning that additional information does not reduce further the uncertainty of the parameter at this point.
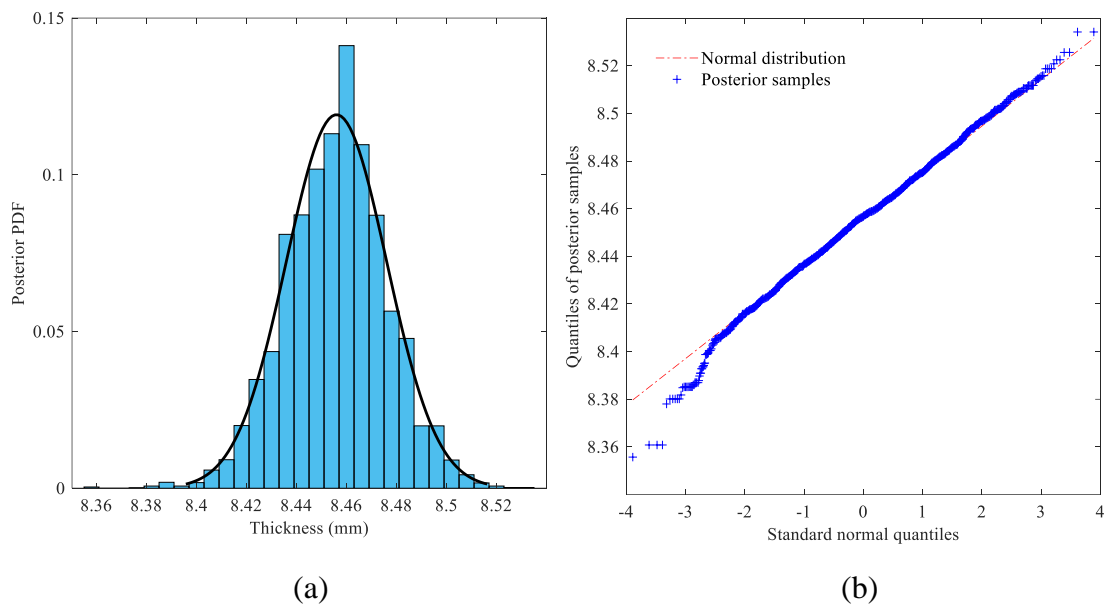

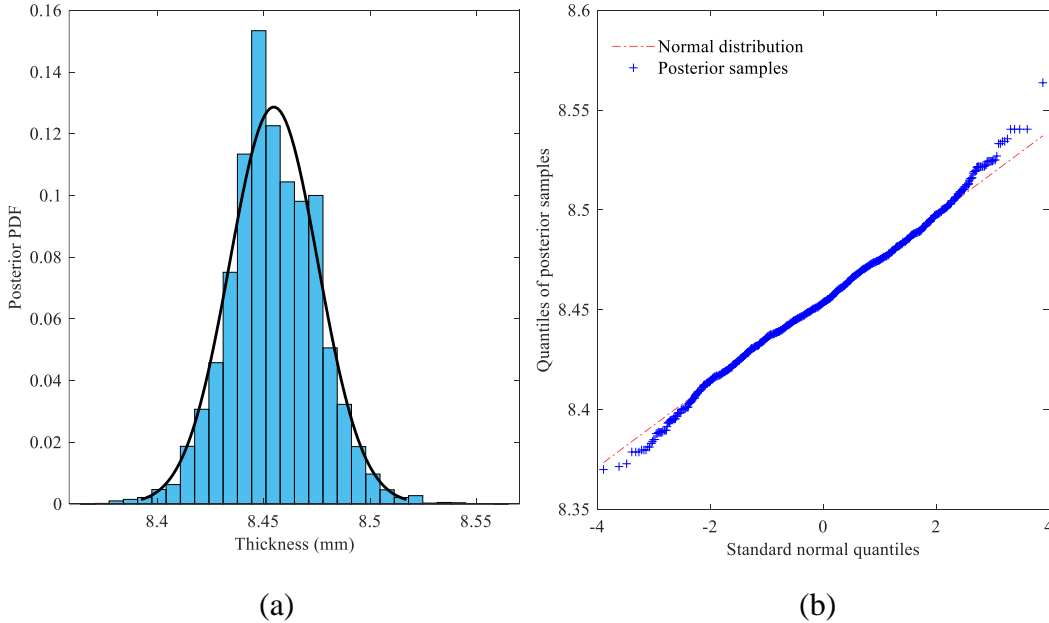(a)   (b)

Figure 6.6:(a) Histogram of the posterior distribution of thickness for the optimal sensor under stochastic operational conditions, (b) corresponding Q-Q plot. (Normal Prior).

Table 6.2: Parameter estimations for the optimal sensor under stochastic operational conditions. (Normal Prior).

Parameter	Target Value	Point Estimate	% Difference	Credible Interval
t (mm)	8.47	8.450	0.23	[8.41, 8.49]
σ (με)	5	-		-

6.2.3 Outlier Behavior

It is important to highlight that the aforementioned results, occurred for load instances that are considered relatively usual to occur, namely, these are load instances where the parameters $q_0, \bar{x}, \bar{y}$ are outcomes of the random variables $Q_0, \bar{X}, \bar{Y}$ from distribution areas that are not further than -2σ and $+2\sigma$. However, it is also critical to explore the respective results from load realizations that do not fall in these areas, and thus to describe the behavior of the system in outlier conditions. These outlier conditions occur when at least two of the parameters $q_0, \bar{x}, \bar{y}$ are outcomes of the random variables $Q_0, \bar{X}, \bar{Y}$ from distribution areas further than -2σ and $+2\sigma$. Employing the uninformative uniform prior, the results shown in Figure 6.7 and Table 6.3 are

generated. The chain has converged to a stationary distribution which is approximated by a normal distribution; however, this distribution does not contain the thickness' target value, hence the estimations of the parameter are considered inaccurate. As a next step, the biased normal prior was also employed, and results are presented in Figure 6.8 and Table 6.4 respectively. Based on these results, in order for the system to proceed to good and valid estimations for the thickness parameter under outlier operational conditions, a biased prior is required. It is also noted that the uncertainty interval is wider compared to the cases of the previous section. Furthermore, load instances that are described by the parameters $q_0, \bar{x}, \bar{y}$ from distribution areas further than -3σ and $+3\sigma$, set the marginalized likelihood to zero and MCMC algorithm can't be performed.

(a)   (b)

Figure 6.7:(a) Histogram of the posterior distribution of thickness, (b) corresponding Q-Q plot. (Outlier behavior with uniform prior).

Table 6.3 Parameter estimations for the optimal sensor under stochastic operational conditions. (Outlier behavior with uniform prior).

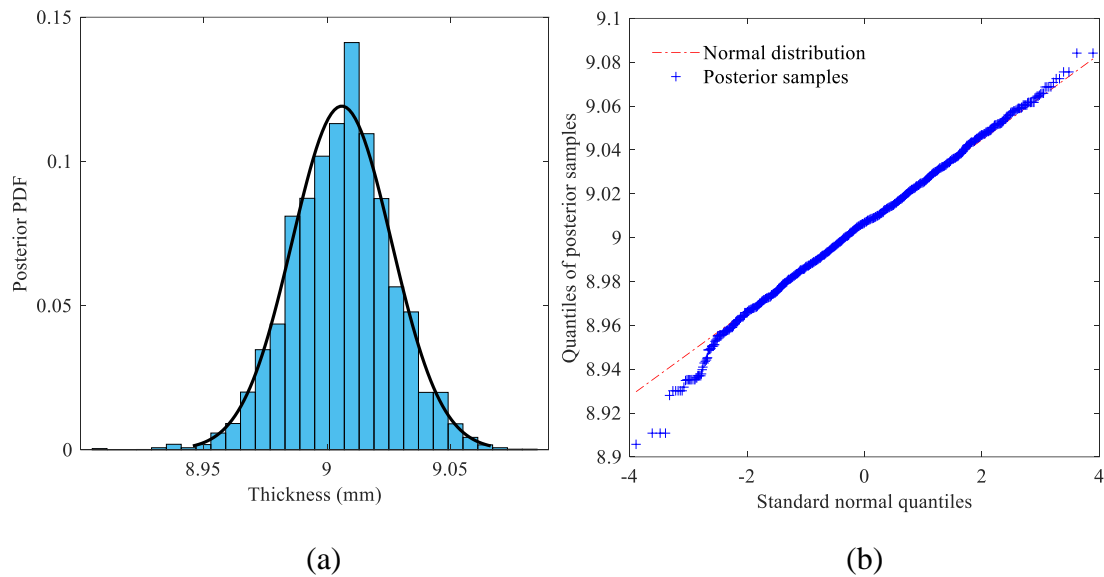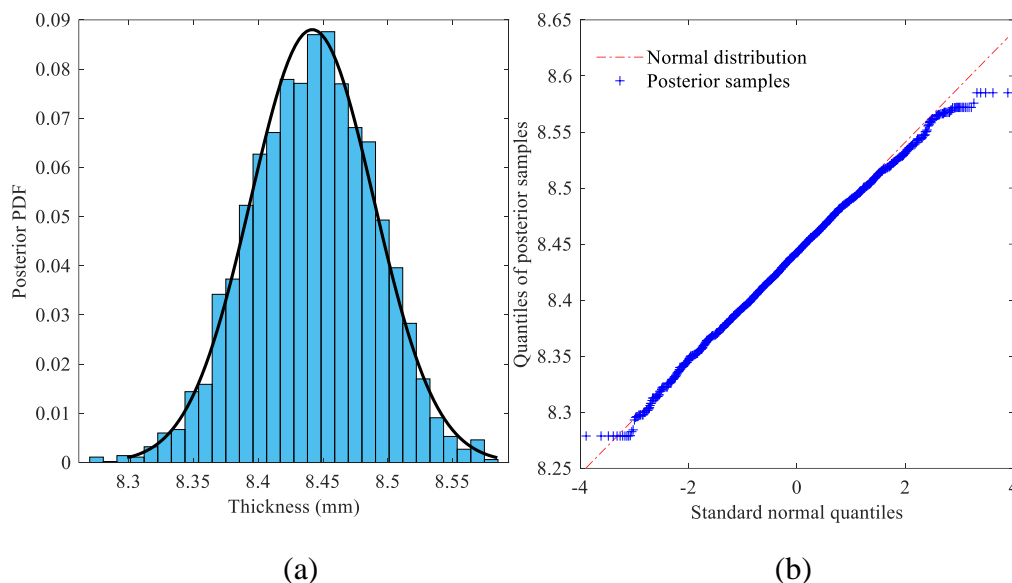| Parameter	Target Value	Point Estimate	% Difference	Credible Interval
t (mm)	8.47	9.00	6.26	[8.96, 9.04]
σ (με)	5	-		-

(a)   (b)

Figure 6.8:(a) Histogram of the posterior distribution of thickness, (b) corresponding Q-Q plot. (Outlier behavior with normal prior).

Table 6.4: Parameter estimations for the optimal sensor under stochastic operational conditions. (Outlier behavior with normal prior).

Parameter	Target Value	Point Estimate	% Difference	Credible Interval
t (mm)	8.47	8.50	0.35	[8.34, 8.54]
σ (με)	5	-		-

In an attempt to overcome outlier issues a different observation data set was also tested. Thus far strain measurements were generated from a single unknown operational condition described by the random variables $Q_0, \bar{X}, \bar{Y}$ and by adding the effect of noise. However, in the current attempt, strain measurements will be generated from different operational conditions along with an added noise outcome of the residual probabilistic model and will be considered as the observations within the Bayesian and MCMC process. In such manner, results are extracted by taking into account multiple and possible outlier conditions. Figure 6.9 illustrated the trace plot of the generated chain, while Figure 6.10 illustrates the generated thickness posterior distribution. In addition, Table 6.5 contains the corresponding numerical results. The chain appears to move around the target thickness adequately based on the trace plot, and through the created posterior distribution good point estimations and relatively narrow credible interval are obtained.
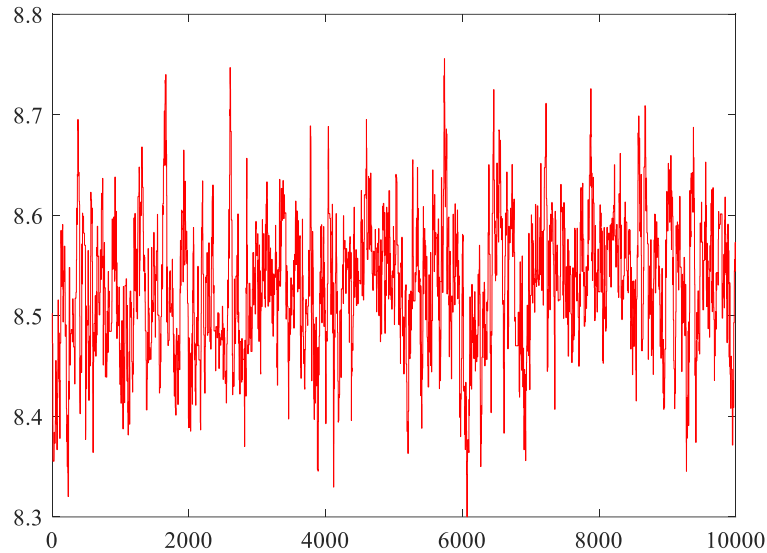
Figure 6.9: Trace plot showing the trajectory of the chain based on the new data set.
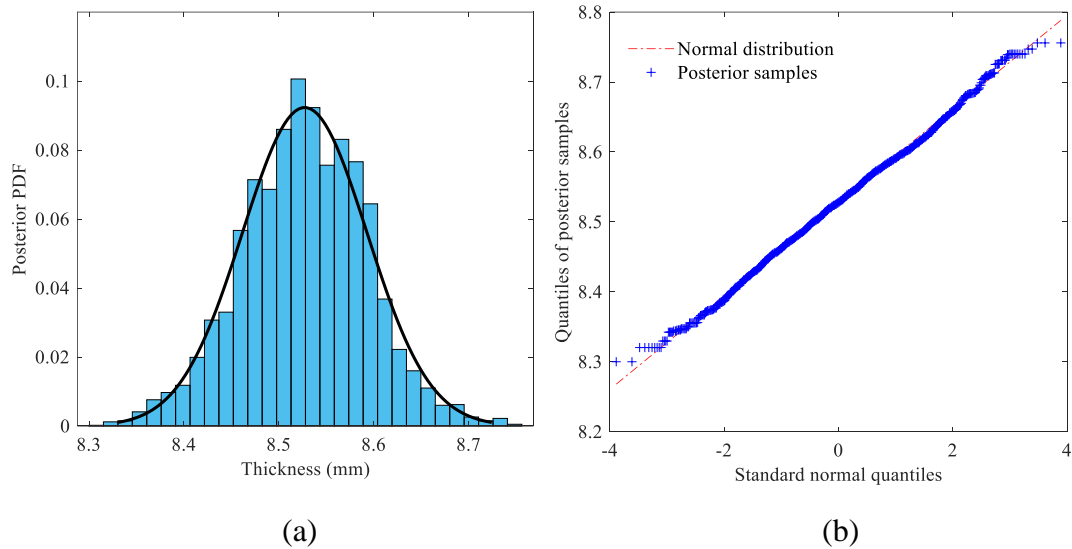

(a)	(b)

Figure 6.10: (a) Histogram of the posterior distribution of thickness for the optimal sensor under stochastic operational conditions based on the new data system, (b) corresponding Q-Q plot.

Table 6.5: Parameter estimations for the optimal sensor under stochastic operational conditions base in the new data set system.

Parameter	Target Value	Point Estimate	% Difference	Credible Interval
t (mm)	8.47	8.47	0	[8.39, 8.65]
σ (με)	5	-		-

Nonetheless, after illustrating the correlogram of this case in Figure 6.11, it became obvious that the autocorrelation between samples has not decayed to zero even at lag number 50. Therefore, the generated samples are considered highly correlated resulting in biased estimation of the parameter of thickness. This signifies that for such a case, a larger number of samples is necessary to be generated in order to achieve asymptotic independence.
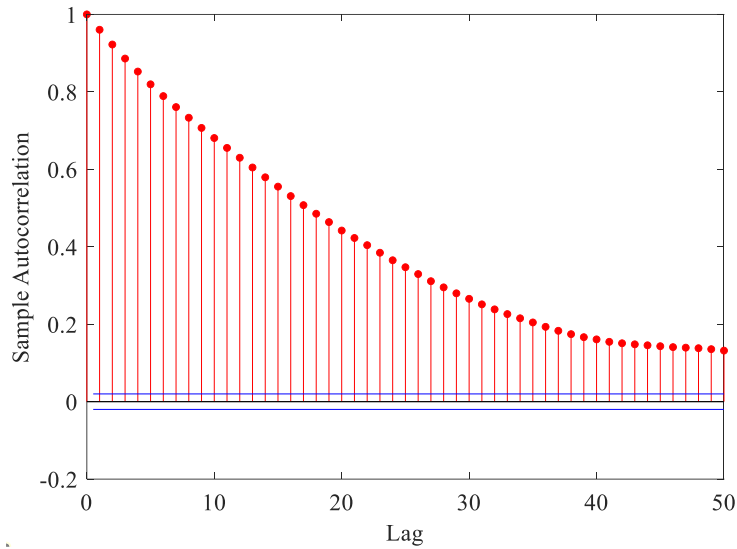
Figure 6.11: Correlogram for the parameter of thickness based on the new data set.

6.2.4 The Noise Level Effect

The aforementioned results were generated for a standard deviation level σ of 5 με. However, it is essential to examine what is the effect of different noise levels on the estimation of the thickness parameter. Towards this direction, the MCMC process was performed for higher noise levels of 10 με and 20 με respectively. The results are illustrated and compared in the following figures. It can be observed that the more the noise level increases, the slower the correlation between samples decays to zero. For the highest noise level of 20 με, the correlation is extremely high even at large number of lags. The chain is not mixed appropriately (Figure 6.12) and no valid estimations can be made. At such a high noise level, the system requires a significantly larger number of generated samples in order to achieve asymptotic independence. With respect to the noise level of 10 με, a higher correlation between samples is observed but within acceptable limits. Hence, one can proceed to parameter estimation as shown in Table 6.6, where the % difference between point estimate and target value is significantly increased compared to the noise level of 5 με, and the uncertainty interval appears wider.
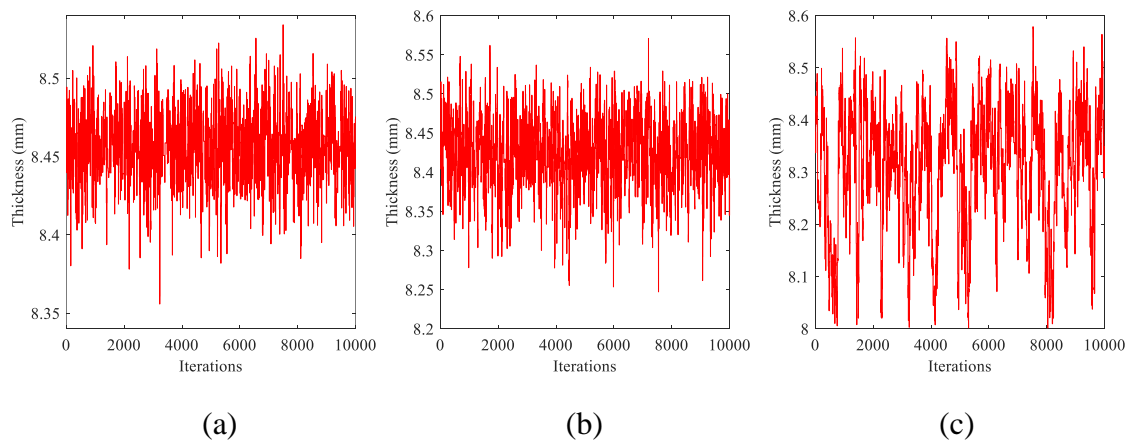

(a)   (b)   (c)

Figure 6.12: Trace plots for different noise levels, (a) 5 με, (b) 10 με, (c) 20 με.
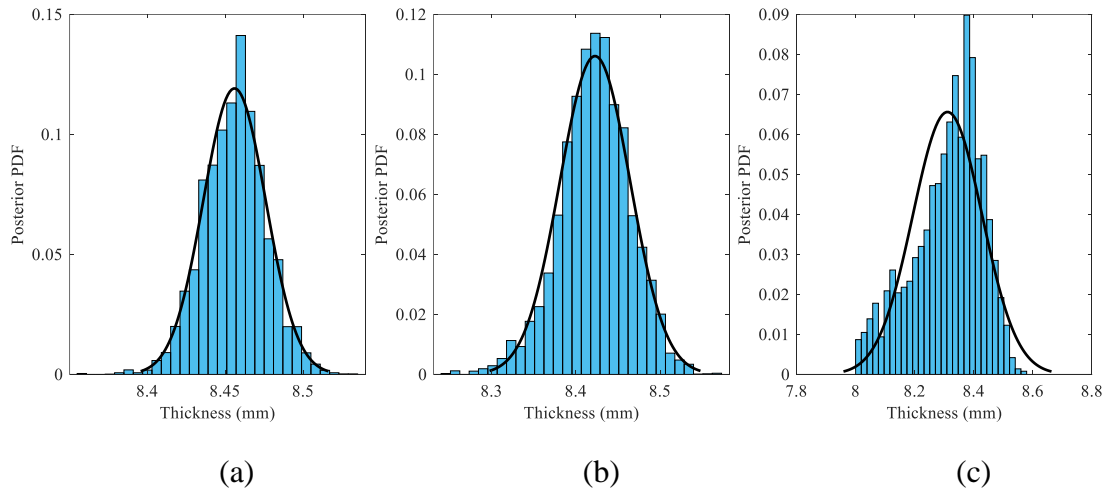
Figure 6.13: Posterior distributions of thickness for different noise levels, (a) 5 µε, (b) 10 µε, (c) 20 µε.
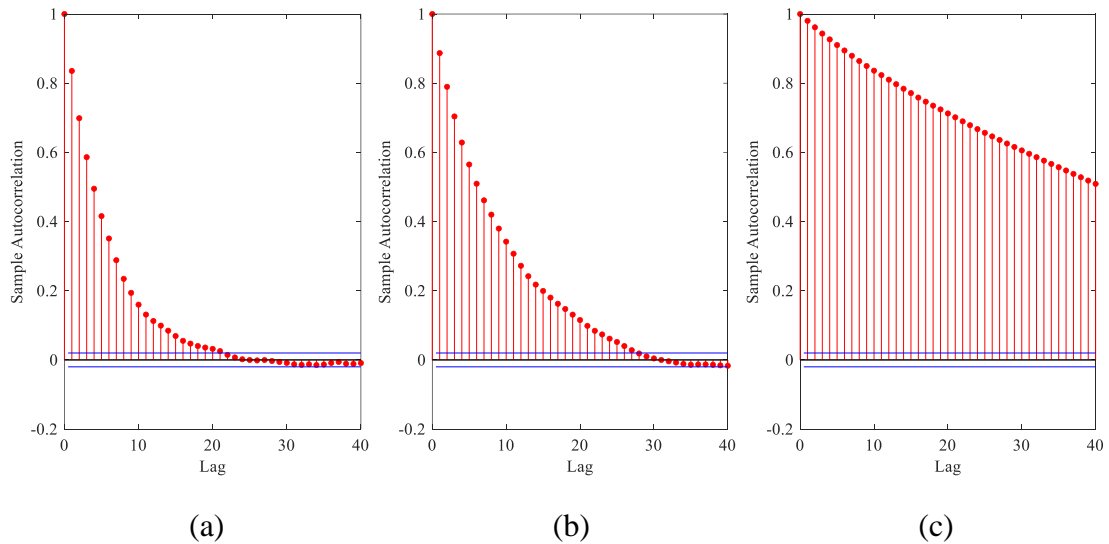
Figure 6.14: Correlograms for different noise levels (a) 5 µε, (b) 10 µε, (c) 20 µε.

Table 6.6: Parameter estimations for noise level of 10 µε.

Parameter	Target Value	Point Estimate	% Difference	Credible Interval
t (mm)	8.47	8.40	0.83	[8.34, 8.50]
σ (µε)	5	-		-

6.3 Deterministic Operational Conditions

Respectively, results with regard to deterministic operational conditions are presented in this section.

6.3.1 Convergence Diagnostics and Autocorrelation

Similar to the case of stochastic operational conditions Figure 6.15 illustrates the trace plots of the chains for both parameters. In the current case it is observed that all chains for both parameters have mixed, each having reached the unique corresponding stationary distribution. The chains are moving adequately fast, and they are exploring the entire sample space around the true values of the targeted parameters. It should be noted that the acceptance rate in this case reaches 42%. Moreover, Figure 6.16 illustrates the ACF graphs for both parameters, where it is clear that sample autocorrelation decays to zero quickly at short lags. Generally speaking, the created chain behaves better under deterministic operational conditions, with a higher acceptance rate and the ability to make estimations for both unknown parameters.

(a)   (b)
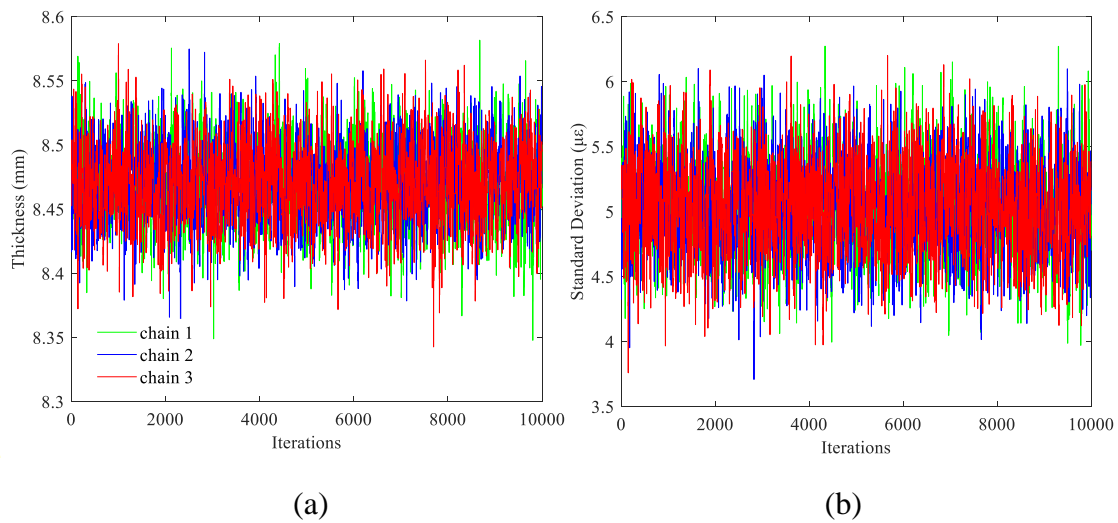
Figure 6.15: Trace plots showing the trajectory of the chains under deterministic operational conditions, for the parameter of (a) thickness and (b) standard deviation.
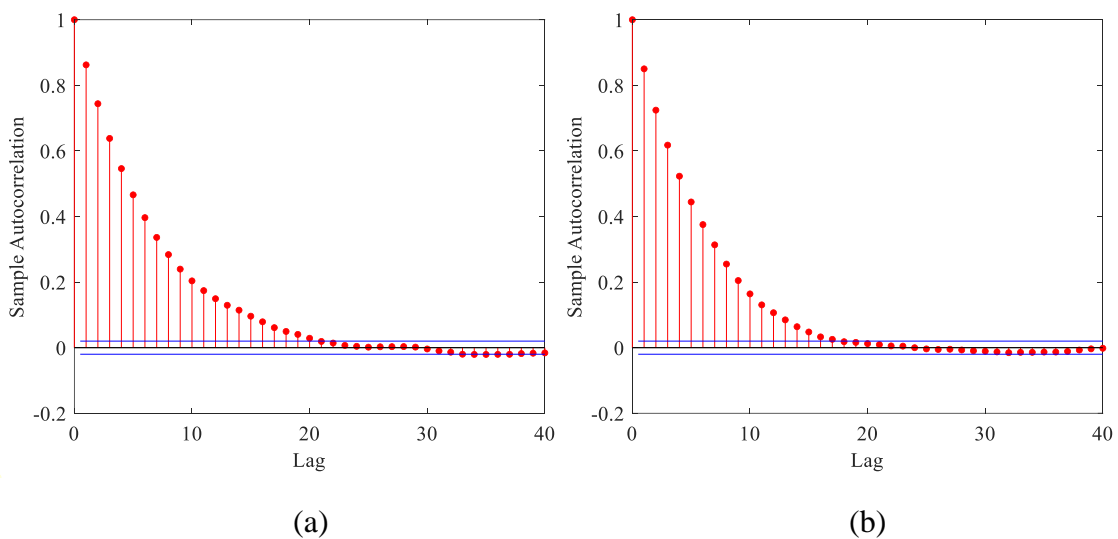

(a)   (b)

Figure 6.16: Correlogram under deterministic operational conditions, for the parameter of (a) thickness and (b) standard deviation.

6.3.2 Marginal Posterior Distributions

Based on the aforementioned, one can proceed to the marginal posterior distributions in order to make point estimations and credible intervals for the QoI. Figure 6.17 and Figure 6.18 illustrate the marginal posterior distributions for the thickness and standard deviation parameter respectively, when uninformative uniform prior is employed. Both parameters' distributions can be approximated again by utilizing normal distributions. The corresponding estimations are presented in Table 6.7. It is observed that under deterministic operational conditions, Bayesian estimations are very close to the targeted values for both parameters with an associated narrow uncertainty 95% interval. Also, it should be noticed that estimations do not deviate much from the corresponding estimations under stochastic operational conditions with usual loading instances.

(a)   (b)
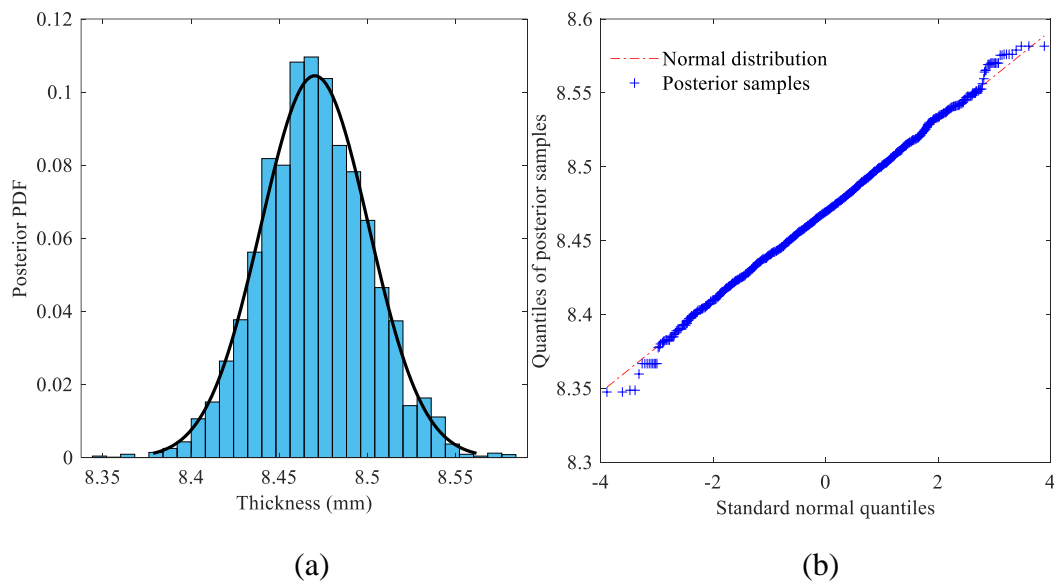
Figure 6.17: (a) Histogram of the posterior distribution of thickness under deterministic operational conditions, (b) corresponding Q-Q plot. (Uniform Prior).
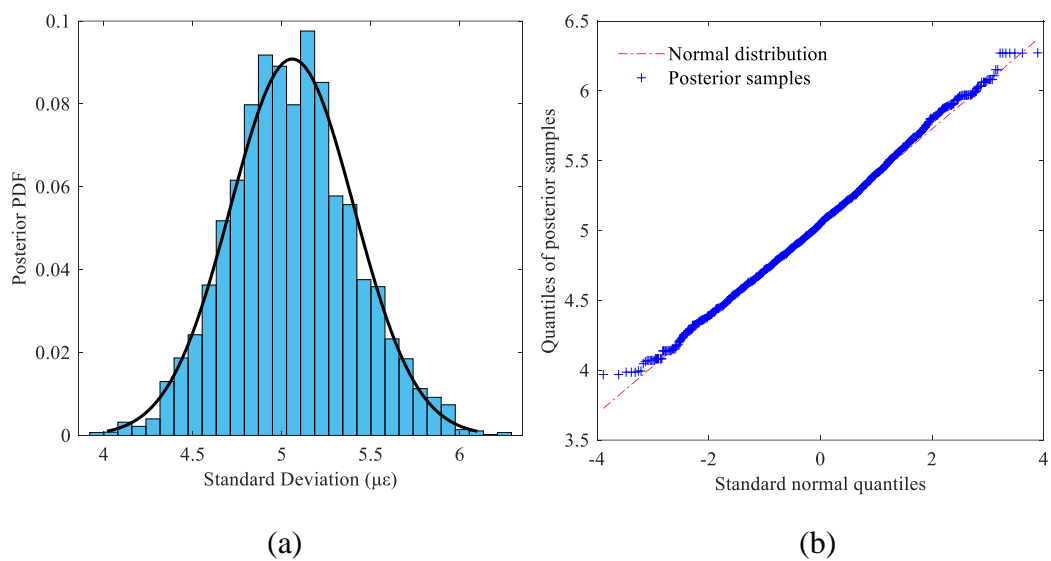

(a)   (b)

Figure 6.18: (a) Histogram of the posterior distribution of standard deviation under deterministic operational conditions, (b) corresponding Q-Q plot. (Uniform Prior).

Table 6.7: Parameter estimations for the optimal sensor under deterministic operational conditions. (Uniform Prior).

Parameter	Target Value	Point Estimate	% Difference	Credible Interval
t (mm)	8.47	8.47	0	[8.41, 8.52]
σ (με)	5	5.13	2.6	[4.36, 5.75]

To further assess if parameter uncertainty with respect to the thickness of the plate can be further reduced, the biased normal prior was employed. Results are presented in Figure 6.19 and Table 6.8 respectively. However, it is observed that the behavior is almost identical to when the uniform prior distribution was employed, thus no additional knowledge can further reduce thickness uncertainty.
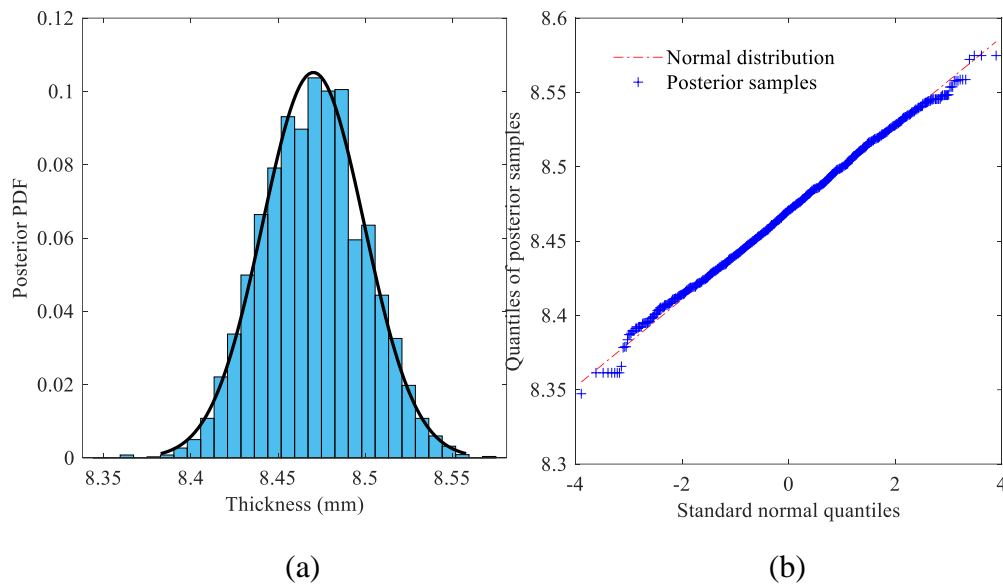
Figure 6.19: (a) Histogram of the posterior distribution of standard deviation under deterministic operational conditions, (b) corresponding Q-Q plot. (Normal Prior).

Table 6.8: Parameter estimations for the optimal sensor under deterministic operational conditions. (Uniform Prior).

Parameter	Target Value	Point Estimate	% Difference	Credible Interval
t (mm)	8.47	8.48	0.12	[8.42, 8.52]
σ (με)	5	5.13	2.6	[4.36, 5.75]

7 Concluding Remarks

The goal of the present study was to investigate a SHM system for parameter estimation and uncertainty quantification of the thickness of a plate domain in a uniformly corroded state, under both stochastic and deterministic operational conditions utilizing Bayesian inference. Strain measurements from sensors on the plate were considered as observation data. The implementation of the method was carried out in a numerical setting, through MCMC Metropolis algorithm and by using high-fidelity FE model and surrogate modeling to generate the strain response data. Different sources of uncertainty affecting the strain measurements in both operational conditions were considered to appropriately construct a probabilistic model in the Bayesian framework. The key findings of the employed research are listed below:

- Sensor locations and strain components that appear to have the highest strain response are considered optimal for data collection because they are affected less by measurement noise.
- Under stochastic operational conditions and for load instances that are relatively usual to occur, Bayesian estimations are very close to the targeted values regarding the thickness parameter. However, the system fails to make estimations about the residual parameter σ that describes measurement discrepancies in the constructed probabilistic model.
- Under stochastic operational conditions the system does not behave well in outlier loading instances when no prior biased knowledge is available. Only when biased prior probability distribution is employed together with large number of generated samples, are Bayesian estimations unbiased and close to the real target values.
- As measurement noise level increases, parameter uncertainty as well as sample correlation also increases. Sample correlation increases up to a point where no valid estimations can be developed, and a significantly larger number of samples is essential to achieve asymptotic sample independence.
- Under deterministic operational conditions, the Bayesian system provides good estimations and narrow uncertainty intervals for both thickness and standard deviation parameter with no significant deviation from the stochastic case in usual loading conditions.

The performance of Bayesian inference in thickness estimation of a plate subjected to uniform corrosion encourages the expansion of this application in a more complex framework like crack identification. The number of quantities of interest in such cases increases as now one is interested in the location of the crack, the crack's length as well as the cracks orientation. The increased dimensionality of such problems poses serious constraints regarding the FE model, the surrogate models and the MCMC methodologies that are employed to deal with Bayesian inference. Most likely, conventional MH algorithm will not be appropriate and advanced and complicated MCMC methods, like Hamiltonian Monte Carlo will be necessary.

8 References

[1] "International Association of Classification Societies (IACS), "Rec76 - IACS Guidelines for Surveys, Assessment and Repair of Hull Structure - Bulk Carriers," 1994. [Online].Available: https://iacs.org.uk/publications/recommendations/61-80/".

[2] "International Association of Classification Societies (IACS),"Common Structural Rules for Double Hull Oil Tankers and Bulk Carriers," 2022. [Online]. Available:https://iacs.org.uk/publications/common-structural-rules/csr-for-bulk-carriers-and-oil-tankers/".

[3] D. P. a. D. Tsiourva, Διάβρωση Και Προστσία Σε Θαλάσσιες Και Μηχανολογικές Κατασκευές (Ακαδημαϊκές Σημειώσεις) [Corrosion and Protection in Marine and Mechanical Structures (Academic Handouts)], School of Naval Architecture and MarineEngineering, Athens: NTUA 2012.

[4] "Hess, P., Aksu, S., Vaz, M., Feng, G., Li, L., Jurisic, P., ... & Egorov, A. (2018). Committee V. 7: Structural Longevity. In Proceedings of the 20th International Ship and Offshore Structures Congress (ISSC 2018) Volume 2 (pp. 391-460). IOS Press.".

[5] "Farrar, C. R., Doebling, S. W., & Nix, D. A. (2001). Vibration–based structural damage identification. Philosophical Transactions of the Royal Society of London. Series A: Mathematical, Physical and Engineering Sciences, 359(1778), 131-149.".

[6] "Ahmad, R., & Kamaruddin, S. (2012). An overview of time-based and condition-based maintenance in industrial application. Computers & industrial engineering, 63(1), 135-149.".

[7] "Reifsnider, K., & Majumdar, P. (2013). Multiphysics stimulated simulation digital twin methods for fleet management. In 54th AIAA/ASME/ASCE/AHS/ASC Structures, Structural Dynamics, and Materials Conference".

[8] "Millwater, H., Ocampo, J., & Crosby, N. (2019). Probabilistic methods for risk assessment of airframe digital twin structures. Engineering Fracture Mechanics, 221, 106674.".

[9] "Ben Miled, Z., & French, M. O. (2017). Towards a reasoning framework for digital clones using the digital thread. In 55th AIAA aerospace sciences meeting (p. 0873).".

[10] "R. Bitton et al., "Deriving a cost-effective digital twin of an ics to facilitate security evaluation", in Computer Security, J. Lopez, J. Zhou, and M. Soriano, Eds., Cham:Springer International Publishing, 2018, pp. 533–554".

[11] "Karve, P. M., Guo, Y., Kapusuzoglu, B., Mahadevan, S., & Haile, M. A. (2020). Digital twin approach for damage-tolerant mission planning under uncertainty. Engineering Fracture Mechanics, 225, 106766.".

References

[12] "Glaessgen, E., & Stargel, D. (2012, April). The digital twin paradigm for future NASA and US Air Force vehicles. In 53rd AIAA/ASME/ASCE/AHS/ASC structures, structural dynamics and materials conference.".

[13] "Zhou, C., Xu, J., Miller-Hooks, E., Zhou, W., Chen, C. H., Lee, L. H., ... & Li, H. (2021). Analytics with digital-twinning: A decision support system for maintaining a resilient port. Decision Support Systems, 143, 113496.".

[14] "ABS, Enhancing safety on FPSOs: Leveraging digital technologies, American Bureau of Shipping https://ww2.eagle.org/content/dam/eagle/advisories-and-debriefs/ABS Enhancing Safety on FPSOs Leveraging Digital Technologies.pdf," [Online].

[15] "Nikolaos E. Silionis, Diploma Thesis: " Damage Identification in Thin-walled Girders througa Finite Element-Based Digital Twin." Athens, November 2020".

[16] "Preisler, A., Schröder, K. U., & Schagerl, M. (2018). Intrinsic damage assessment of beam structures based on structural damage indicators. Am J Eng Res, 7(6), 56-70.".

[17] *A. Katsoudas, "Diploma Thesis: Damage Identification in Idealised Geometries Utilising Machine Learning Methods: A theoretical Study"..*

[18] "Rytter, A. (1993). Vibrational based inspection of civil engineering structures.".

[19] "Zhu, B., & Frangopol, D. M. (2013). Incorporation of structural health monitoring data on load effects in the reliability and redundancy assessment of ship cross-sections using Bayesian updating. Structural Health Monitoring, 12(4), 377-392.".

[20] "Silionis, N. E., & Anyfantis, K. N. (2022). Static strain-based identification of extensive damages in thin-walled structures. Structural Health Monitoring, 21(5), 2026-2047.".

[21] "Argyris, C., Chowdhury, S., Zabel, V., & Papadimitriou, C. (2018). Bayesian optimal sensor placement for crack identification in structures using strain measurements. Structural Control and Health Monitoring, 25(5), e2137.".

[22] "Silionis, N. E., & Anyfantis, K. N. (2022, June). On the detection of thickness loss in ship hull structures through strain sensing. In European Workshop on Structural Health Monitoring (pp. 207-216). Cham: Springer International Publishing.".

[23] "Yao, Y., Yang, Y., Wang, Y., & Zhao, X. (2019). Artificial intelligence-based hull structural plate corrosion damage detection and recognition using convolutional neural network. Applied Ocean Research, 90, 101823.".

[24] "Falcetelli, F., Yue, N., Di Sante, R., & Zarouchas, D. (2022). Probability of detection, localization, and sizing: The evolution of reliability metrics in Structural Health Monitoring. Structural Health Monitoring, 21(6), 2990-3017.".

References

[25] "Martinez-Luengo, M., Kolios, A., & Wang, L. (2016). Structural health monitoring of offshore wind turbines: A review through the Statistical Pattern Recognition Paradigm. Renewable and Sustainable Energy Reviews, 64, 91-105.".

[26] T. Dodwell, "https://www.digilab.co.uk/news/understanding-uncertainty-quantification-different-types-of-uncertainty," [Online].

[27] "Lee, S. H., & Chen, W. (2009). A comparative study of uncertainty propagation methods for black-box-type problems. Structural and multidisciplinary optimization, 37, 239-253.".

[28] "Zhang, J. (2021). Modern Monte Carlo methods for efficient uncertainty quantification and propagation: A survey. Wiley Interdisciplinary Reviews: Computational Statistics, 13(5), e1539.".

[29] "Nagel, J. B. (2019). Bayesian techniques for inverse uncertainty quantification. IBK Bericht, 504.".

[30] "Tikhonov, A. N., Goncharsky, A. V., Stepanov, V. V. E., Yagola, A. G. E., Tikhonov, A. N., Goncharsky, A. V., ... & Yagola, A. G. (1995). Numerical methods for the approximate solution of ill-posed problems on compact sets (pp. 65-79). Springer Netherland".

[31] "Stuart, A. (2010). Inverse problems: A Bayesian perspective. Acta Numerica, 19, 451-559. doi:10.1017/S0962492910000061".

[32] "Freedman, D. (1995). Some issues in the foundation of statistics. Foundations of".

[33] "Myung, I. J. (2003). Tutorial on maximum likelihood estimation. Journal of mathematical Psychology, 47(1).".

[34] "Akaike, H. (1998). Likelihood and the Bayes procedure (pp. 309-332). Springer New York.".

[35] "Ayyub, B. M. (2001). Elicitation of expert opinions for uncertainty and risks. CRC press.".

[36] "Ghosh, M. (2011). Objective priors: An introduction for frequentists, pp. 187-202.".

[37] "Diaconis, P., & Ylvisaker, D. (1979). Conjugate priors for exponential families. The Annals of statistics, pp. 269-281.".

[38] "Fortini, S., & Ruggeri, F. (2000). On the use of the concentration function in Bayesian robustness. Robust Bayesian Analysis, pp. 109-126.".

[39] "Tibshirani, R. (1996). Regression shrinkage and selection via the lasso. Journal of the Royal Statistical Society Series B: Statistical Methodology, 58(1), pp. 267-288.".

References

[40] "Hespanhol, L., Vallio, C. S., Costa, L. M., & Saragiotto, B. T. (2019). Understanding and interpreting confidence and credible intervals around effect estimates. Brazilian journal of physical therapy, 23(4), 297-301.".

[41] "Metropolis, N., & Ulam, S. (1949). The monte carlo method. Journal of the American statistical association, 44(247), pp. 335-341.".

[42] "G. Aravanis, "Diploma Thesis: Construction of Data-Driven Models for the Identification of Large-Scale Damages in Stiffened Panel Geometries", Athens, May 2023, pp. 9-11.".

[43] "Robert, C. P., Casella, G., Robert, C. P., & Casella, G. (1999). Monte carlo integration. Monte Carlo statistical methods, 71-138.".

[44] "Norris, J. R. (1998). Markov chains (No. 2). Cambridge university press.".

[45] William M. Bolstad (2010): "Computational Bayesian Statistics", pp.106-109.

[46] "Martin Haugh (2017): Lecture Notes on MCMC and Bayesian Modeling, pp.5-6".

[47] "Haario, H., Saksman, E., & Tamminen, J. (1999). Adaptive proposal distribution for random walk Metropolis algorithm. Computational statistics, 14, 375-395.".

[48] "Taboga, Marco (2021). "Markov Chain Monte Carlo (MCMC) diagnostics", Lectures on probability theory and mathematical statistics. Kindle Direct Publishing. Online appendix. https://www.statlect.com/fundamentals-of-statistics/Markov-Chain-Monte-Carlo-diagno".

[49] "Vivekananda Roy (2019): "Convergence diagnostics for Markov chain Monte Carlo"".

[50] "https://www.researchgate.net/publication/228608614_Markov_chain_Monte_Carlo-based_approaches_for_inference_in_computationally_intensive_inverse_problems".

[51] "Gelman, A., Carlin, J.B., Stern, H.S., Dunson, D.B., Vehtari, A., & Rubin, D.B. (2013). Bayesian Data Analysis (3rd ed.). Chapman and Hall/CRC. https://doi.org/10.1201/b16018".

[52] "Zhou, Z. H. (2021). Machine learning. Springer Nature.".

[53] "Cristiani, D., Sbarufatti, C., & Giglio, M. (2021). Damage diagnosis and prognosis in composite double cantilever beam coupons by particle filtering and surrogate modelling. Structural Health Monitoring, 20(3), 1030-1050.".

[54] "Bhattacharyya, T., Singh, S. B., Dey, S. S., Bhattacharyya, S., Bleck, W., & Bhattacharjee, D. (2013). Microstructural prediction through artificial neural network (ANN) for development of transformation induced plasticity (TRIP) aided steel. Materials Sc".

References

[55] "Miller, S. J. (2006). The method of least squares. Mathematics Department Brown University, 8, 1-7.".

[56] "Awad, M., Khanna, R., Awad, M., & Khanna, R. (2015). Support vector regression. Efficient learning machines: Theories, concepts, and applications for engineers and system designers, 67-80.".

[57] "Smola, A. J., & Schölkopf, B. (2004). A tutorial on support vector regression. Statistics and computing, 14, 199-222.".

[58] "Ying, X. (2019, February). An overview of overfitting and its solutions. In Journal of physics: Conference series (Vol. 1168, p. 022022). IOP Publishing.".

[59] "Wu, Q., & Zhou, D. X. (2005). SVM soft margin classifiers: linear programming versus quadratic programming. Neural computation, 17(5), 1160-1187.".

[60] "de Souza, D. A. C., Ribeiro Filho, S. L. M., de Carvalho, A. L. C., Silva, N. S., Barcelos, S. M., & Christoforo, A. L. (2013). Topological Optimization and Genetic Algorithms Used in a Wheel Project for a Drone.".

[61] "IDEA StatiCa, "CBFEM Weld Model: Validation and Verification," IDEA StatiCa, [Online].," [Online].

[62] P. A. Caridis, Finite Element Method and Applications on thin-walled structures (Accademic Handouts)-Υπολογιστικές Μέθοδοι και Εφαρμογές σε Λεπτότοιχες Κατασκευές (Ακαδημαϊκές Σημειώσεις), School of Naval Architecture and Marine Engineering, NTUA.

[63] "Zienkiewicz, O. C., & Taylor, R. L. (2005). The finite element method for solid and structural mechanics. Elsevier.".

[64] K. Anyfantis, Στατικη Ναυπηγικών Κατασκευων (Πανπιστημιακεσ Σημειωσεις)[Static Structural Mechanics of Marine Structures [Academic Handouts]]-School of Naval Architecture and Marine Engineering-National Technical University of Athens,2020.

[65] "Ivošević, Š., Meštrović, R., & Kovač, N. (2017). An approach to the probabilistic corrosion rate estimation model for inner bottom plates of bulk carriers. Brodogradnja: Teorija i praksa brodogradnje i pomorske tehnike, 68(4), 57-70.".